Consequences of Short Term Mobility Across Heterogeneous Risk Environments:

The 2014 West African Ebola Outbreak

by

Baltazar Espinoza Cortes

A Dissertation Presented in Partial Fulfillment
of the Requirements for the Degree
Doctor of Philosophy

Approved March 2018 by the
Graduate Supervisory Committee:

Carlos Castillo-Chávez, Chair
Yun Kang
Muntaser Safan

ARIZONA STATE UNIVERSITY

May 2018

ABSTRACT

In this dissertation the potential impact of some social, cultural and economic factors on Ebola Virus Disease (EVD) dynamics and control are studied. In Chapter two, the inability to detect and isolate a large fraction of EVD-infected individuals before symptoms onset is addressed. A mathematical model, calibrated with data from the 2014 West African outbreak, is used to show the dynamics of EVD control under various quarantine and isolation effectiveness regimes. It is shown that in order to make a difference it must reach a high proportion of the infected population. The effect of EVD-dead bodies has been incorporated in the quarantine effectiveness. In Chapter four, the potential impact of differential risk is assessed. A two-patch model without explicitly incorporate quarantine is used to assess the impact of mobility on communities at risk of EVD. It is shown that the overall EVD burden may lessen when mobility in this artificial high-low risk society is allowed. The cost that individuals in the low-risk patch must pay, as measured by secondary cases is highlighted. In Chapter five a model explicitly incorporating patch-specific quarantine levels is used to show that quarantine a large enough proportion of the population under effective isolation leads to a measurable reduction of secondary cases in the presence of mobility. It is shown that sharing limited resources can improve the effectiveness of EVD effective control in the two-patch high-low risk system. Identifying the conditions under which the low-risk community would be willing to accept the increases in EVD risk, needed to reduce the total number of secondary cases in a community composed of two patches with highly differentiated risks, has not been addressed. In summary, this dissertation looks at EVD dynamics within an idealized highly polarized world where resources are primarily in the hands of a low-risk community – a community of lower density, higher levels of education and reasonable health services – that shares a "border" with a high-risk community that lacks minimal resources to survive an EVD outbreak.

ii

Para mi esposa Ana Rosa de la Mora Moret; gracias por acompañarme, apoyarme y soportarme, siempre con amor, alegría y paciencia durante nuestro camino juntos, cuanto me has enseñado.

Para mi hijo Baltazar Espinoza de la Mora; cada día me enseñas a ser papá y a ser hijo, eres una fuente infinita de amor, alegría, inspiración y motivación desde que llegaste a mi vida.

Para mi hijo Daniel Espinoza de la Mora; mamá, papá y tu hermano, esperan con ansias recibirte y compartir la alegría de estar juntos, eres una fuente infinita de amor, alegría, inspiración y motivación.

Para mi padre Baltazar Espinoza Tintos; gracias por todas las enseñanzas que me has brindado y tu apoyo incondicional, me enseñaste que nada es imposible si de verdad se desea, gracias por ser mi mejor amigo.

Para mi madre Ninfa Sofia Cortes Carrillo; gracias por tanto amor, me has enseñado a disfrutar y cuidar las cosas importantes de la vida, siempre me escuchas y soportas mis rabietas con paciencia.

Para mi tío Daniel Cortes Carrillo[†]; siempre me apoyaste incondicionalmente, me enseñaste con tu ejemplo que la vida es para disfrutarse en todo momento, hasta donde estés.

Para mi familia; cada uno de ustedes me han enseñado a siempre buscar ser mejor persona, gracias por todas las memorias.

ACKNOWLEDGMENTS

Many people have strongly influenced me over my professional career, without all their motivation and advisory I would never reached this point. My first adviser was my own father, who sowed the seed of Mathematics in me. By continuously challenging me with puzzles when I was a kid, he taught me that I can have fun doing mathematics and I am still having tons of fun. My first experiences in mathematical contests and research with Prof. Ulises Omar Candelario Velázquez, showed me the exciting experience of being part of the Mathematics community. He taught me the power of cooperative learning and teamwork. Dr. Ricardo Alberto Sáenz Casas at the University of Colima, taught me the rigorous mathematics involved in doing research. He introduced me to a fractional dimension world while writing my undergraduate thesis. Dr. Carlos Castillo-Chávez gave me the opportunity to participate in the Mathematical and Theoretical Biology Institute (MTBI) 2011, an experience that changed my life. He helped me to break my own limits and always encouraged me to exploit my full potential during my graduate career. I continue expanding my own frontiers and outwitting my limits under his advisory. I also would like to thank Dr. Fred Brauer, Dr. Yun Kang, Dr. Anuj Mubayi, Dr. Muntaser Safan, Dr. Sherry Towers, Dr. Derdei Bichara and Dr. Adam Lampert, for their advisory during my graduate student period, all their invaluable teachings and their patience. I also thank my friends and colleagues Victor Moreno, Juan Renova, Diego Chowell, Komi Messan, Daniel Burkow, Fereshteh Nazari, Jordan Bates, Michael Lin and Dustin Padilla.

TABLE OF CONTENTS

LIST OF TABLES

LIST OF FIGURES

Chapter 1

INTRODUCTION

This dissertation aims to understand the potential impact of some social, cultural and economic factors on Ebola Virus Disease (EVD) dynamics and control. Differences in such factors are assumed across regions within the community of interest, thus defining distinct environments (or patches) with specific risks of infection. Individuals moving across these patches experience different infection risks over time. The assumed risk variation plays a determinant role by adjusting the disease impact over the whole community. In absence of specialized treatment or an approved vaccine against EVD, understanding how risk variations across environments reduces or increases the number of EVD secondary cases is critical to refine existent control strategies.

Discovered in the late 1970's, Ebolavirus (EBOV) was identified as the culprit for two outbreaks: in Zaire (now the Congo) and the Sudan, where the EVD (formerly known as Ebola hemorrhagic fever) startled the international community (Johnson et al., 1977; Bowen et al., 1977; Commission et al., 1978). This new virus showed an astonishing ability to transmit among humans as well as strikingly high mortality rates (ranging from 50% to 90%) (WHO, 2015). Such elevated fatality rates are the result of its capacity to attack almost every tissue in the human body (except lymphocytes), by invading cells trhough different mechanisms (Falasca et al., 2015). EBOV is a genus of the Filoviridae family causing severe symptoms, differentiated into two phases: the first phase is mainly characterized by headache, fever, diarrhea and severe weakness; while the second phase is driven by a functional failure of the liver and kidneys, producing internal and external bleeding through body orifices (WHO, 2015; Nelson and Williams, 2013). The virus is transmitted during the second symptoms phase, through direct contact with bodily fluids of infected and

EVD-infected corpses; through semen, breast milk and other bodily secretions (Feldmann and Geisbert, 2011; CDC, 2018e,d). Recent studies showed that recovered individuals still possess the Ebolavirus for several days during convalescence (Chughtai et al., 2016; Deen et al., 2017). EBOV can also be sexually transmitted long after the acute illness phase. In fact, after the 2014-2016 EVD outbreak, a new virus resurgence was linked to sexual transmission by a recovered patient, more than 500 days after symptoms onset (Diallo et al., 2016).

The EVD is a zoonotic disease, meaning that it can spread across species. EVD has been found in gorillas, monkeys, fruit bats and humans (Feldmann and Geisbert, 2011; CDC, 2018d). Currently, the EVD natural reservoir is not known, but, there is evidence suggesting the fruit bat as the most likely wild reservoir (Pourrut et al., 2005; Feldmann et al., 2004). Its zoonotic nature makes eradication through control programs (for instance, the case of smallpox eradication (Breman et al., 1980)) difficult, if not impossible, to achieve. Consequently, the disease can remain undetected in a wild reservoir for years until the next spillover occurs. After the Zaire and Sudan outbreaks, there have been 24 EVD outbreaks, most of them occurring in Central Africa (WHO, 2015). These outbreaks had the common characteristic of arising in small, rural communities where the EVD was self-contained (Coltart et al., 2017). The deadliest and worst outbreak was the 2014 West African epidemic, caused by the Ebola virus (EBOV, formerly designated Zaire ebolavirus, which is the most dangerous of the *Ebolavirus* genus), and was responsible for approximately 28,600 cases and more than 11,000 deaths (CDC, 2018a; Kuhn et al., 2010; Gire et al., 2014). It is suspected the virus spread from Central Africa, where the EVD is considered endemic, and started the 2014 West African outbreak through a single zoonotic event in Guinea (Feldmann et al., 2004; Baize et al., 2014). The new outbreak rapidly propagated from Guinea to Liberia in March and to Sierra Leone in May 2014 (UN, 2018; Gire et al., 2014; CDC, 2018a).

In response to the rapidly increasing outbreaks, a few weeks after EVD reached Lagos, Nigeria (the most populous city in Africa), on August 1st 2014, governments decided to implement *cordons sanitaires* on the region containing at the time more than 70% of the epidemic (Agence France-Presse, 2018). During this period, military force was used to prevent individuals from traveling outside the cordoned area. This control strategy was aimed to limit the spread of the disease, but not focused on improving or maintaining conditions within the cordoned zone. The imposed traveling curtailments produced a humanitarian crisis. The food transportation system was seriously affected, to the point that individuals inside the highly affected region suffered from scarcity, lack of appropriate health care and increased risk of infection (Amesh Adalja, 2018; R. K. Hoffmann et.al, 2018). Despite efforts to control population trying to escape from the cordoned region, some people found ways to outwit the *cordons sanitaires* (ONISHI, 2014). This in turn reflected an increased effective reproduction number and an increased amount of cases (Towers et al., 2014; Espinoza et al., 2016; Pandey et al., 2014). These results, suggest that the traveling restriction might have accelerated the contagion process and that *cordons sanitaires* might not be an effective control measure.

Despite massive efforts to control the spread of the EVD epidemic, the virus reached the large cities of Monrovia, Freetown and Conakry, increasing the risk of international spread (UN, 2018; Gomes et al., 2014). In July 2014, Sierra Leone was declared in a state of emergency, followed by Liberia and Guinea in August, 2014 (UN, 2018). On August 8th 2014, the World Health Organization declared Ebola an international health emergency (BBC News, 2018). Besides outbreak containment, another major challenge also emerged. It was shown that during the West African outbreak, the rate of observed EBOV genetic variation duplicated the mutation rate between outbreaks (Gire et al., 2014). Such variations have the potential to produce EBOV functional changes and stressed the importance of competent public health strategies to quickly control an EVD outbreak.

The overall goal in this dissertation is to shed light on how mobility and social factors like insufficient health-care infrastructure, unsafe traditional burial practices, proximity between highly vulnerable areas and big cities, and delayed international responses, promoted the progression of local outbreaks to an international public health threat. In Chapter 2, the inability to detect and isolate a large fraction of EVD-infected individuals before symptoms onset is addressed. A mathematical model calibrated with data from the 2014 West African outbreak scenario is used to show the dynamics of EVD control under various quarantine effectiveness regimes. The proposed model, focuses on studying the impact of current technology allowing early detection of infected individuals up to three days before symptoms appear on the EVD dynamics. The presented model incorporates secondary infections produced by infected and quarantined individuals, and secondary infections produced by EVD-infected corpses. My findings are in agreement to current literature results where the impact of early detection without explicitly incorporate infections produced by EVD-infected corpses was addressed (Chowell et al., 2015). Massive quarantine of pre-symptomatic individuals would lead to the effective management of EVD, provided high enough quarantine effectiveness. The impact of average EVD-infected corpses removal periods on the quarantine effects is assessed.

Chapter 3 provides a short review of some approaches used in metapopulation models. Particularly, the modeling framework used in the construction of the multi-patch models in subsequent Chapters 4 and 5 is described (Bichara et al., 2015; Castillo-Chavez et al., 2016). In Chapter 4, a two-patch model based on the single patch model presented in Chapter 2, without explicitly incorporating quarantine, is studied. The impact of mobility across neighboring regions exhibiting differential risk of EVD infection is studied. By a single parameter, health services, access inequalities and resources are modeled.

In this model, one patch is calibrated to resemble infection risk conditions similar to those within the *cordons sanitaires* region during the 2014 West African outbreak; the sec-

ond patch is assumed to experience a lower risk of infection and is incapable of sustaining an epidemic. It is shown that population mobility might increase or reduce the total number of secondary cases generated. Furthermore, the effects of the population density ratio on the efficiency of the *cordons sanitaires* are studied. Results show that the *cordons sanitaires* does not always minimize the final epidemic size; moreover, high mobility regimes have the potential to reduce an EVD outbreak. In Chapter 5, a model explicitly accounting for patch-specific quarantine levels is used to study the joint effects of mobility and early detection of infected individuals on regions exhibiting highly distinct risks of infection. Naturally, quarantine implementation reduces the traveling regime needed to ameliorate the impact of an EVD outbreak through mobility. However, the harmful effect of massive quarantine programs (by reducing the *effective population* traveling) might play an adverse role on the overall control of EVD in the presence of mobility. Finally, in Chapter 6, present work implications and challenges to improve current global sensitivity to worldwide epidemics are discussed.

Chapter 2

THE IMPACT OF QUARANTINE CAPACITY AND ISOLATION EFFECTIVENESS
ON THE EVD DYNAMICS

2.1   Introduction

The lack of a vaccine or effective treatment for Ebola Virus Disease (EVD), along to its
relatively high contagiousness, implied that EVD transmission was likely best controlled
by isolating patients and the use of barriers on health-care workers (Matua et al., 2015;
CDC, 2018b). Even under specialized health care, approximately 50% to 90% of EVD
infected individuals die (CDC, 2018a; Bruce and Brysiewicz, 2002). Current health aid to
EVD-infected individuals consists of providing early supportive care maintaining hydration
and blood pressure levels (WHO, 2015; Ansumana et al., 2015), postexposure treatments
have also been studied, however there are none currently approved (Feldmann, 2010). Cur-
rent development of a highly effective vaccine seems promising; nonetheless, systematic
implementation aimed to ameliorate a possibly new Ebola outbreak requires more research
on the side effects (A. Maxmen, 2017; E. Callaway, 2017).

EVD is transmitted as a result of contact with infected bodily fluids and, it is already
recognized as a potential bioterrorism agent (Feldmann and Geisbert, 2011; Borio et al.,
2002; CDC, 2017). Based on the small number of suspected infected cases by airborne
transmission, it cannot be conclusively excluded. Nonetheless, droplet and aerosol spread
routes of transmission have been evaluated in efforts to weaponize the Ebola virus (Polesky
and Bhatia, 2003). More recently it has been confirmed that a survivor can sexually transmit
the Ebola virus for a period of more than 500 days after symptoms onset (Diallo et al.,
2016).

Since the majority of Ebola cases have been the result of human-to-human transmission (Gire et al., 2014), effective isolation has critical importance in containing an outbreak. Currently, efforts to control EVD mostly rely on isolation strategies and good sanitation techniques when dealing with both sick and dead contaminated individuals (Pandey et al., 2014). EVD diagnosis is challenging during the early stages of infection. The symptoms caused are similar to those of Marburg virus, Typhoid fever, Plague, Yellow fever and Chikungunya fever among others (Feldmann and Geisbert, 2011). EVD identification is done through laboratory diagnosis, thus demanding high specialized human resources and infrastructure. Currently there are two main assays to diagnose Ebola infection, focusing on detecting particle components in infected individuals (RT-PCR) and measuring the host immune response (ELISA) (Feldmann and Geisbert, 2011). Particularly, RT-PCR assays offer the possibility of detecting Ebola infection up to three days before symptoms onset (Towner et al., 2004). Previous work studying the consequences of early diagnosis of infected individuals found that early diagnosis combined with effective isolation leads to a rapid reduction of Ebola transmission (Chowell et al., 2015). This work resemble conditions found on developed countries, where exposure to infected dead bodies is minimal and this transmission route can be neglected.

The goal of this project is to understand the impact of misinformation, cultural practices and resource limitations on the complex disease dynamics exhibited during the EVD 2014 West African outbreak. The heroic actions done by health-care workers adequately managing the spread of EVD in Lagos, Nigeria was a milestone in the control of the West African EVD outbreak. However, this poses a critical question: what are the minimal requirements to control an EVD outbreak? For instance, for an EVD outbreak happening in a large urban center, like Lagos (densely comparable to New York city), using current diagnostic technology (RT-PCR) to help determine up to three days in advance whether an individual has been infected with EVD, what levels of quarantine and isolation effectiveness are required

in order to control an outbreak? or, what is the impact of properly handling EVD-induced dead bodies?

This chapter is organized as follows. In section 2.2, I present an ODE based mathematical model to describe a population's progression through the EVD contagion process. Section 2.3 is devoted to analyze the proposed model, computing the associated basic reproductive number and final epidemic size relation. Results and simulations addressing the aforementioned questions are presented in section 2.4. Finally, in section 2.5 the consequences of the obtained results are highlighted as well as work limitations.

2.2 Model Derivation

The population studied is assumed to be constant and divided into Susceptible (S), latent undetectable individuals (E_1), latent detectable individuals (E_2), infected individuals (I), quarantined infected individuals (Q), EVD-infected corpses (D) and removed individuals: recovered individuals and properly buried dead bodies (R). The total population (including dead individuals) is then $N = S + E_1 + E_2 + I + Q + D + R$. The contagion process decreases the susceptible population by infections due to contacts between infected individuals (I), quarantined infected individuals (Q) or EVD-infected corpses (D), with susceptible individuals (S), at rate $\beta \left(\frac{I + \varepsilon D + lQ}{N} \right)$. Latent individuals are assumed to be detectable via RT-PCR test on average $\frac{1}{\kappa_1}$ days after being infected, and become infectious on average after a period of $\frac{1}{\kappa_1} + \frac{1}{\kappa_2}$ days. During the second latency stage ($\frac{1}{\kappa_2}$ days before symptoms onset), a fraction q of pre-symptomatic individuals are diagnosed and taken to isolation, while the rest are neither detected nor isolated. Non-isolated infected individuals might die with probability f_d or recover after a mean period of $\frac{1}{\gamma}$ days. Until removed, on average after $\frac{1}{v}$ days, dead bodies are assumed capable to produce new infections. During this period, since EVD dead bodies (D) have the highest viral load, they are assumed to be more infectious than infected individuals, ($\varepsilon > 1$). Finally, quarantined infected individuals

8

are assumed to have a reduced infectious rate ($l < 1$), and recover or die after a mean period of $\frac{1}{\gamma}$ days. Quarantined EVD induced deaths are assumed to be safely buried immediately, not contributing to the infectious process.

During the West African Ebola outbreak asymptomatic individuals associated with low viral loads were detected via PCR test (Leroy et al., 2000). Supporting antecedents of patients with symptoms ranging from mild, severe and rapid fatality can be found, for instance during the Sudan (1976) and Zaire (1979) outbreaks (of a WHO/International Study Team et al., 1978). Asymptomatic individuals are not explicitly modeled in this work due to association with low viral loads and the secondary infections produced by this subpopulation are neglected.

Population's transitions through the EVD disease stages are showed in Figure 2.1
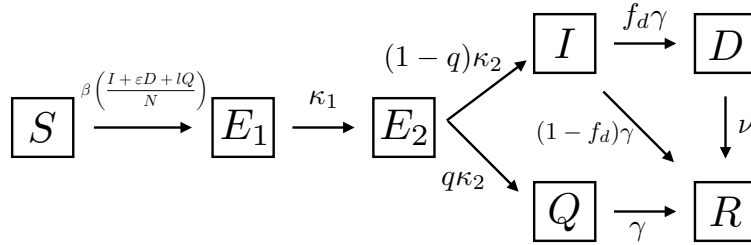
Figure 2.1: Ebola compartmental model with quarantine intervention.

and mathematically described by the system of ordinary differential equations (2.1)

$$
\begin{cases}
N = S + E_1 + E_2 + I + Q + D + R \\
\dot{S} = -\beta S \left(\frac{I + \varepsilon D + lQ}{N} \right) \\
\dot{E}_1 = \beta S \left(\frac{I + \varepsilon D + lQ}{N} \right) - \kappa_1 E_1 \\
\dot{E}_2 = \kappa_1 E_1 - \kappa_2 E_2 \\
\dot{I} = (1-q)\kappa_2 E_2 - \gamma I \\
\dot{Q} = q\kappa_2 E_2 - \gamma Q \\
\dot{D} = f_d \gamma I - \nu D \\
\dot{R} = (1-f_d)\gamma I + \nu D + \gamma Q
\end{cases}
\tag{2.1}
$$

9

The parameters used in this work are directly extracted from literature. It is estimated from previous EVD outbreaks a mean period from symptoms onset to end of infectiousness $\left(\frac{1}{\kappa}\right)$ of 7 days (Legrand et al., 2007; Ndambi et al., 1999). The infected dead bodies burial mean period (bodies infectious period) is approximately 2 days (Legrand et al., 2007); while fatality rate of EVD is on average 70% (Team, 2014). Since high viral load has been associated with high fatality rates, in the present work infectiousness of EVD-induced dead bodies is assumed greater than the one of infected individuals, that is, $\varepsilon > 1$ (Li et al., 2016). The parameter β has been approximated to calibrate model's (2.1) basic reproduction number to $\mathscr{R}_0 \approx 2.45$ (Althaus, 2014; Chowell et al., 2004). Quarantine capacity (q) and isolated individuals' relative infectiousness (l) are varied on the range $[0,1]$ in order to explore the whole spectrum effects on the EVD dynamics. Table 2.1, summarize the parameters used in this research.

Table 2.1: Parameters of the single patch EVD model.

Parameter	Description	Base model values	
β	Per susceptible infection rate	0.287	(Althaus, 2014)
γ	Rate at which an infected recovers or dies	1/7	(Team, 2014)
κ_1	Per-capita progression rate to latent detectable stage	1/4	(Legrand et al., 2007)
κ_2	Per-capita progression rate from latent detectable to infectious stage	1/3	(Towner et al., 2004)
ν	Per-capita body disposal rate	1/2	(Legrand et al., 2007)
f_d	Proportion of infected who die due to infection	0.7	(Team, 2014)
ε	Scale: Ebola infectiousness of EVD-infected corpses	> 1	(Li et al., 2016)
q	Proportion of latent individuals diagnosed before symptoms onset	[0,1]	
l	Isolated individuals relative transmissibility	[0,1]	

2.3 Model Analysis

2.3.1 Computation of the Control and Basic Reproductive Numbers

System's (2.1) control and basic reproduction numbers are computed by following the next generation approach (Diekmann et al., 1990; van den Driessche and Watmough, 2002).

Consider model's (2.1) infected subpopulations, i.e. E_1, E_2, I, Q and D. By evaluating model (2.1) at the disease free equilibrium, $S = N$ and

$$F = \begin{pmatrix} 0 & 0 & \beta & l\beta & \varepsilon\beta \\ 0 & 0 & 0 & 0 & 0 \\ 0 & 0 & 0 & 0 & 0 \\ 0 & 0 & 0 & 0 & 0 \\ 0 & 0 & 0 & 0 & 0 \end{pmatrix} \quad \text{and} \quad V = \begin{pmatrix} \kappa_1 & 0 & 0 & 0 & 0 \\ -\kappa_1 & \kappa_2 & 0 & 0 & 0 \\ 0 & -(1-q)\kappa_2 & \gamma & 0 & 0 \\ 0 & -q\kappa_2 & 0 & \gamma & 0 \\ 0 & 0 & -f_d\gamma & 0 & v \end{pmatrix}.$$

The control reproduction number $\mathscr{R}_c$, quantify the number of secondary infections caused by a single infected individual in a totally susceptible population, under the effects of control measures. The $\mathscr{R}_c$ is the spectral radius of the next generation matrix

$$-FV^{-1} = \begin{pmatrix} q\left(\frac{l\beta}{\gamma}\right) + \beta(1-q)\left(\frac{1}{\gamma} + \frac{f_d\varepsilon}{v}\right) & q\left(\frac{l\beta}{\gamma}\right) + \beta(1-q)\left(\frac{1}{\gamma} + \frac{f_d\varepsilon}{v}\right) & \beta\left(\frac{f_d\varepsilon}{v} + \frac{1}{\gamma}\right) & \frac{l\beta}{\gamma} & \frac{\beta\varepsilon}{v} \\ 0 & 0 & 0 & 0 & 0 \\ 0 & 0 & 0 & 0 & 0 \\ 0 & 0 & 0 & 0 & 0 \\ 0 & 0 & 0 & 0 & 0 \end{pmatrix},$$

this is

$$\mathscr{R}_c = q\left(\frac{l\beta}{\gamma}\right) + (1-q)\beta\left(\frac{1}{\gamma} + \frac{f_d\varepsilon}{v}\right). \tag{2.2}$$

The control reproductive number determines the beginning of the recognition of the epidemic. In counterpart, the basic reproductive number $\mathscr{R}_0$ represents the number of secondary infections produced by an infected individual in an essentially susceptible population, in absence of control measures. By writing (2.2) in terms of the secondary infectious produced by quarantined and non-quarantined individuals as follows

$$\mathscr{R}_c = q\mathscr{R}_Q + (1-q)\mathscr{R}_0 \tag{2.3}$$

it is possible to define the quarantine reproductive number $\mathscr{R}_Q = \frac{l\beta}{\gamma}$, which captures the secondary infections produced by a typical individual in quarantine and the basic reproductive number $\mathscr{R}_0 = \beta\left(\frac{1}{\gamma} + \frac{f_d\varepsilon}{v}\right)$, which captures the secondary infections produced by

11

infected individuals and non-removed infected dead bodies in absence of control measures. Explicitly, the control reproductive number $\mathscr{R}_C$, accounts for the secondary infections produced by the proportion (q) of pre-symptomatic individuals diagnosed, during its infectious period $\left(\frac{1}{\gamma}\right)$ at a reduced infectiousness rate $(l\beta)$, secondary infections produced by non isolated infectious individuals during their infectious period $\left(\frac{1-q}{\gamma}\right)$ and secondary infections produced by non-quarantined EVD dead bodies $((1-q)f_d)$ with increased infectiousness rate $(\varepsilon\beta)$ during its average disposal time $\left(\frac{1}{v}\right)$.

2.3.2 Derivation of the Final Epidemic Size

Since the total population of model (2.1) is constant, it is possible to reduce the system to

$$
\begin{cases}
N = S + E_1 + E_2 + I + Q + D + R \\
\dot{S} = -\beta S \left(\frac{I + \varepsilon D + lQ}{N}\right) \\
\dot{E}_1 = \beta S \left(\frac{I + \varepsilon D + lQ}{N}\right) - \kappa_1 E_1 \\
\dot{E}_2 = \kappa_1 E_1 - \kappa_2 E_2 \\
\dot{I} = (1-q)\kappa_2 E_2 - \gamma I \\
\dot{Q} = q\kappa_2 E_2 - \gamma Q \\
\dot{D} = f_d \gamma I - v D
\end{cases}
\tag{2.4}
$$

by assuming $S(0) = N$, $E_1(0) = E_2(0) = I(0) = D(0) = 0$ and using the notation $\hat{f}(t) = \int_0^\infty f(s)ds$ and $f^\infty = \lim_{t\to\infty} f(t)$; from the first two equations of system (2.4), $\dot{S} + \dot{E} = -\kappa_1 E_1 \leq 0$, which implies $E_1^\infty = 0$. Similarly it is possible to get $E_2^\infty = I^\infty = Q^\infty = D^\infty = 0$. By integrating model's (2.4) first two equations, $S^\infty - N = \kappa_1 \hat{E}_1$ which implies $\hat{E}_1 = \dfrac{N - S^\infty}{\kappa_1}$. Similar procedure implies $\hat{E}_2 = \dfrac{N - S^\infty}{\kappa_2}$, $\hat{I} = (N - S^\infty)\left(\dfrac{1-q}{\gamma}\right)$, $\hat{Q} = (N - S^\infty)\left(\dfrac{q}{\gamma}\right)$ and $\hat{D} = (N - S^\infty)\left(\dfrac{f_d(1-q)}{v}\right)$. By integrating model's (2.4) first

equation and using previous derivations

$$\log\left(\frac{N}{S^\infty}\right) = \left(1 - \frac{S^\infty}{N}\right)\left(q\frac{l\beta}{\gamma} + (1-q)\beta\left(\frac{1}{\gamma} + \frac{\varepsilon f_d}{v}\right)\right)$$

$$\log\left(\frac{N}{S^\infty}\right) = \left(1 - \frac{S^\infty}{N}\right)\mathscr{R}_C. \tag{2.5}$$

Equation 2.5 is the typical final size relation (Brauer et al., 2001), which in the presented model relates the number of infected individuals at the end of the outbreak, to the secondary infections produced by isolated and non-isolated infectious individuals, and non removed EVD-induced dead bodies. Denote by $s^\infty = \dfrac{S^\infty}{N}$ the proportion of the final susceptible individuals, equation (2.5) yields

$$\log(s^\infty) = (s^\infty - 1)\mathscr{R}_C. \tag{2.6}$$

Letting $y = s^\infty - 1$ denote the proportion of population infected over the course of the epidemic, equation (2.6) becomes

$$y = 1 - \exp[-y\mathscr{R}_c] \tag{2.7}$$

which give us the final proportion of infected individuals, also known as the epidemic attack rate.

2.4   Results

In this section numerical explorations of the impacts of quarantine early detected EVD-infected individuals are shown. The contagion process is assumed to start by the introduction of a single infected individual $I(0) = 1$, into a completely susceptible population $S(0) = 10,000$, where the rest of initial conditions are $Q(0) = D(0) = R(0) = 0$. Infected individuals' disease progression is assumed to follow model (2.1), calibrated by using the parameter values in Table 2.1.

In Section 2.4.1 the effects of different quarantine capacities (q) and isolation effectiveness (l) on the epidemic dynamics, is explored. Section 2.4.2 is devoted to study the role

of the EVD-dead bodies disposal rate (v) on the quarantine effectiveness. In Section 2.4.3 the effects of implementation delay on quarantine are numerically explored via the final epidemic size.

2.4.1   The Role of Quarantine and Isolation Effectiveness

The unprecedented scale of the West African EVD epidemic exposed the hidden danger of weak health systems in highly dense regions (Piot et al., 2014; Fowler et al., 2014). In this Section, the inability to detect and isolate a large fraction of EVD-infected individuals before symptoms onset is addressed. Via numerical explorations, the effects of distinct quarantine levels (assumed constant over the epidemic course), implemented at different isolation effectiveness are studied.

Figure 2.2 shows the EVD attack rate (final proportion of infected individuals) as function of the proportion of quarantined infected individuals. It is shown that even under perfect quarantine $(l = 0)$, epidemic mitigation (when intended only by quarantine) requires to reach at least 60% of the incident population in order to properly manage an Ebola outbreak. Figure 2.2 shows that quarantine effectiveness bellow 50% ameliorates the attack rate, but even detecting the whole incident population is not enough to mitigate the Ebola outbreak. In other words, the impact of a massive quarantine program is not meaningful for "low" quarantine effectiveness is. Figure 2.3 shows the desirable quarantine capacity and quarantine effectiveness in terms of the control reproductive number $\mathscr{R}_C(q, l)$, in order to properly manage an EVD outbreak.
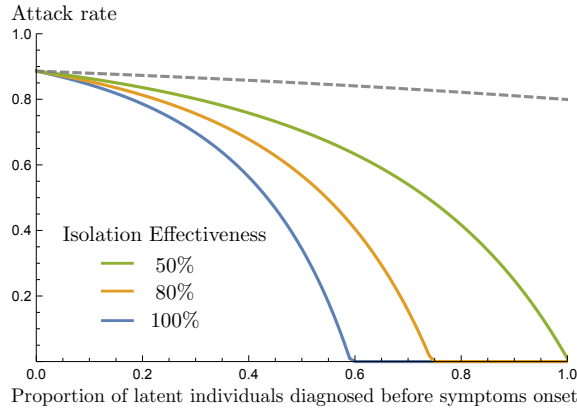
Figure 2.2: EVD attack rate as function of pre-symptomatic diagnosed individuals, for isolation effectiveness $\phi = 80\%, 100\%$ and the extreme case $\phi = 50\%$. The dashed gray line indicates no infectiousness reduction $\phi = 0\%$.
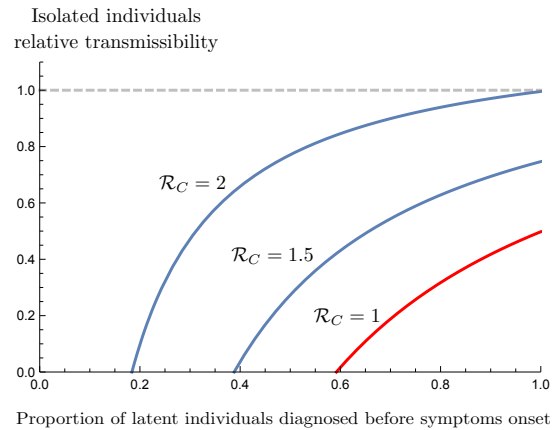
Figure 2.3: Isolation effectiveness of infected individuals as function of the proportion of latent individuals diagnosed before symptoms onset.

Model construction allows to characterize the role of EVD-infected corpses on the final epidemic size under various control scenarios. The gray curve in Figure 2.2 shows the solely impact of properly handle a q proportion of EVD-infected corpses, when quarantine individuals infectiousness is not reduced ($l = 1$). Particularly, under the extreme case when all pre-symptomatic individuals are detected ($q = 1$) and all resulting EVD-infected corpses are properly removed, the attack rate is slightly reduced.

Figure 2.3 shows the level curves of the control reproductive number as function of quarantine capacity and effectiveness, for values $\mathscr{R}_C(q,l) = 2, 1.5$ and the critical threshold $\mathscr{R}_C = 1$. The threshold relation quarantine effectiveness and quarantine capacity is highlighted by the level curve $\mathscr{R}_C = 1$. The pure effect of properly managing EVD-infected corpses, leads the control reproductive number to $\mathscr{R}_C = 2$. This result suggest that at the early stage of the epidemic, each two non-removed EVD-infected corpses produced a new secondary infection during the average removal period. Previous results suggest that quarantine programs can eradicate an Ebola outbreak with the characteristics or the West African epidemic, provided an isolation effectiveness above 50% and whenever at

least 60% of the incident population is quarantined. In order to illustrate this result, Figure 2.4 shows that quarantine of 55% of pre-symptomatic individuals with null infectiousness ($l = 0$) impacts the evolution of the epidemic but is not enough to stop the infectious process. In contrast, Figure 2.5 shows that preventing 60% of pre-symptomatic individuals of producing secondary infections leads to the eventual control of the EVD outbreak.
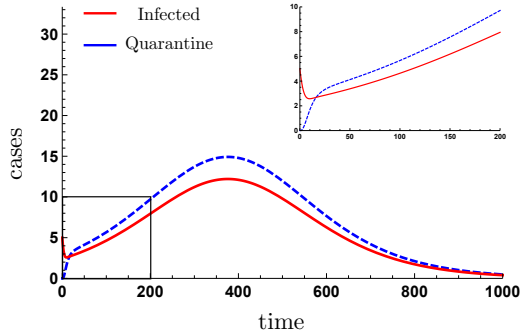
Figure 2.4: Time series of infected and quarantine of 55% pre-symptomatic individuals under perfect isolation ($l = 0$).
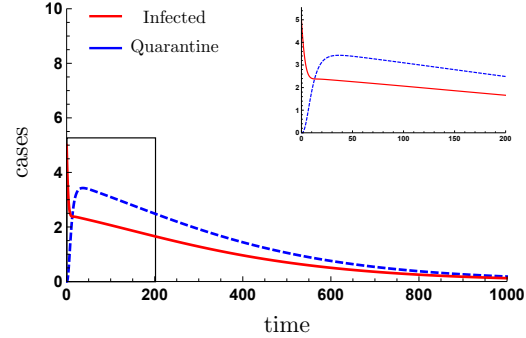
Figure 2.5: Time series of infected and quarantine of 60% pre-symptomatic individuals under perfect isolation ($l = 0$).

From equation (2.3), it is possible derive an expression relating the minimum quarantine capacity required to control an EVD outbreak, given a quarantine effectiveness value

$$q(l) = \frac{1 - \mathscr{R}_0}{\mathscr{R}_Q(l) - \mathscr{R}_0}. \tag{2.8}$$

Figure 2.6 shows the threshold condition $\mathscr{R}_C = 1$ denoting the quarantine capacity and quarantine effectiveness combination needed to control an EVD outbreak.
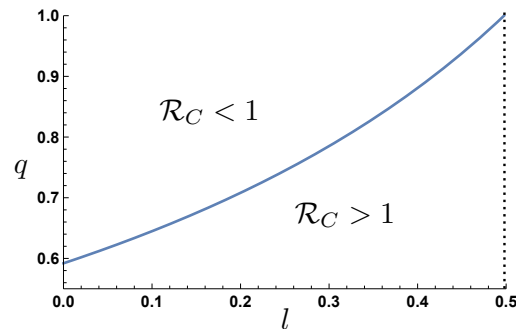
Figure 2.6: Level curve of $\mathscr{R}_C = 1$ on the plane (l, q)

Usually, it is difficult to assess whether increasing quarantine capacity or increasing quarantine effectiveness is the best option in order to enhance sanitary conditions. From equation (2.2), it is possible to characterize the scenarios for which increasing quarantine capacity or increasing isolation effectiveness produces similar impact on reducing the number of EVD secondary cases. This occurs whenever the secondary infections produced by quarantined individuals equals the cumulative secondary infections produced by non quarantined infected individuals and EVD-infected corpses. This is

$$\frac{l\beta}{\gamma} = (1-q)\frac{\beta}{\gamma} + \beta\frac{f_d\varepsilon}{\nu}, \quad \text{which implies} \quad l = 1 - q + \frac{f_d\varepsilon\gamma}{\nu}. \quad (2.9)$$

Figures 2.7 and 2.8, shows the control reproductive number level curves and the attack rate level curves in the (q,l) plane. The red (dashed) line represents the scenarios where augmenting isolation effectiveness produces the same effect that increasing quarantine capacity.
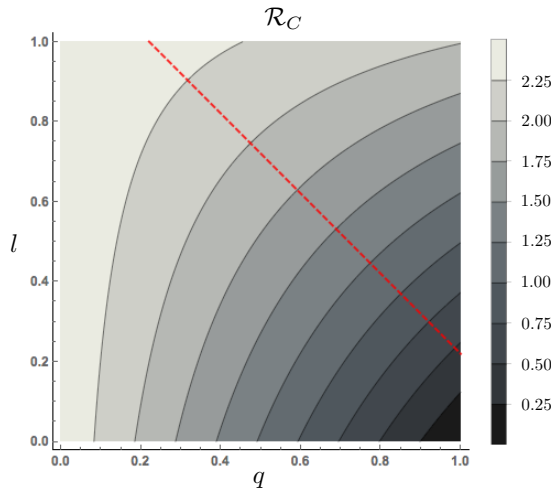
Figure 2.7: Control reproductive number for all quarantine capacities and effectiveness. Along the dashed red curve increasing quarantine capacity reduces $\mathcal{R}_C$ equally than increasing quarantine effectiveness.
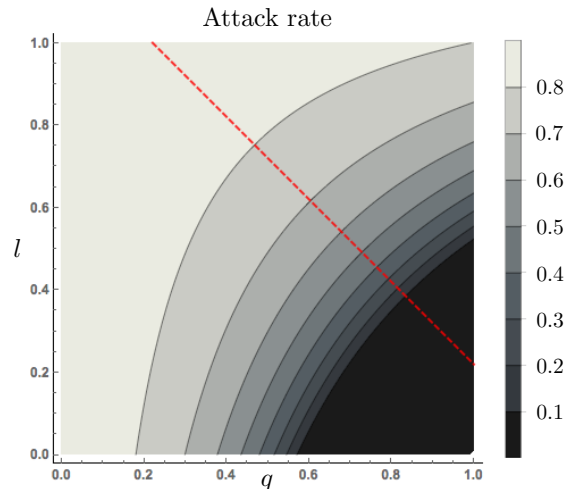
Figure 2.8: Attack rate for all quarantine capacities and effectiveness. Over the red curve increasing quarantine capacity or effectiveness, produces the same reduction of the attack rate.

For $l > 1 - q + \frac{f_d \varepsilon \gamma}{v}$, increasing quarantine effectiveness produces a greater benefit than increase quarantine capacity; while for $l < 1 - q + \frac{f_d \varepsilon \gamma}{v}$ the major benefit is given by increasing quarantine capacity.

Moreover, note that unless quarantine reach at least $\approx 20\%$ of pre-symptomatic individuals, increasing quarantine effectiveness does not produce a significant reduction on the control reproductive number and in consequence the attack rate. This suggest the existence of a tipping point in the relation between quarantine capacity and quarantine effectiveness. More precisely, results suggest that quarantine effectiveness becomes critical provided a minimum quarantine capacity of around 20% of pre-symptomatic individuals is attained.

In summary, according to the presented results, early detection and quarantine of pre-symptomatic infected individuals would mitigate an Ebola outbreak. Nevertheless, EVD mitigation would require extraordinary logistic and coordination efforts. Specifically a quarantine program intending to effectively manage a West African like epidemic would require to isolate a minimum of 60% of early diagnosed infected population. Furthermore, results suggest that without the capacity to isolate at least 20% of pre-symptomatic individuals, increasing isolation effectiveness does not produce substantial benefits.

2.4.2   The Role of EVD-infected Corpses in the Control of EVD

EVD control efforts might not be restricted to guarantee enough quarantine capacity and enough isolation quality. Providing fast removal of EVD-infected corpses substantially helps on breaking transmission chains. During the 2014 West African Ebola outbreak news coverage reported that burial teams capacity were exceeded (ABC News, 2014). Despite of efforts done to persuade communities of avoiding traditional high risk burials, because these had a triggering effect on the spread of EVD, inhabitants continued practicing traditional burial ceremonies to EVD-infected corpses of relatives (Hewlett and Amola, 2003; Piot et al., 2014).

In this section, the role of EVD-infected corpses in the infection process is studied. Particularly, this work focus on addressing how reducing the average removal period of EVD-infected bodies impacts the relationship between quarantine capacity and quarantine effectiveness (equation (2.6)) needed to appropriately manage an EVD epidemic with similar characteristics to the West African scenario.

By equation (2.8), the minimum quarantine needed to eradicate an EVD outbreak depends on both quarantine effectiveness and infected dead bodies removal period. Figure 2.9, shows the relationship between quarantine capacity (q) and quarantine effectiveness (l) required to take $\mathscr{R}_C = 1$, for scenarios when EVD-infected corpses are removed on average after two days, one day and safely removed without exposing susceptible individuals. By reducing susceptible individuals' exposure to EVD-infected corpses the quarantine capacity required to manage an EVD outbreak diminishes. Moreover, the impact of reducing susceptible population's exposure time to EVD-infected corpses increases as quarantine effectiveness improves. Decreasing the critical quarantine capacity of pre-symptomatic infected individuals to 50%, when perfect isolation ($l = 0$) is achieved. Moreover, under quarantine effectiveness bellow the critical 50%, reducing susceptible population's exposure to EVD-infected corpses does not facilitate EVD management.
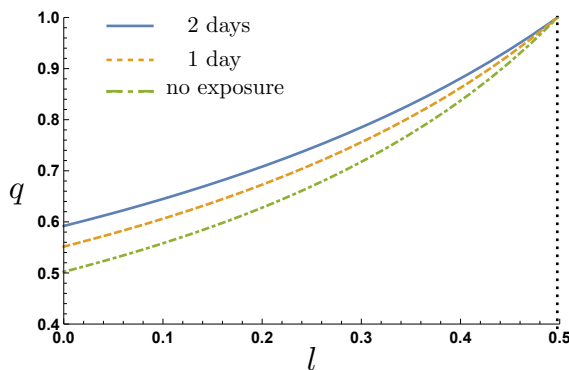
Figure 2.9: The effect of EVD-infected corpses on the quarantine capacity and effectiveness required to properly manage 2014 West African like EVD outbreak.
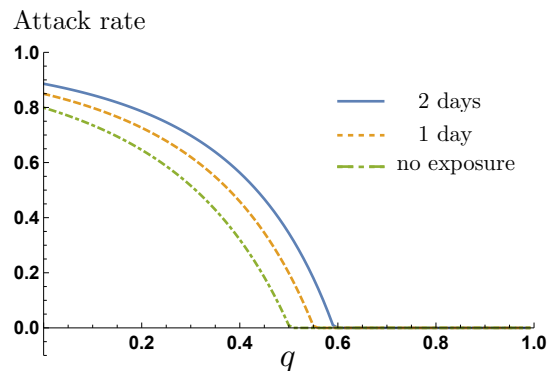
Figure 2.10: Attack rate for infected disposal periods of two days, one day and no exposure.

Figure 2.10 shows that reducing EVD-infected corpses average removal period considerably shift down the attack rate curve, ameliorating the impact of an EVD epidemic and particularly, reducing the minimum quarantine capacity needed to control the West African EVD outbreak.

The presented model calibrated to the West African Ebola outbreak suggest that infected individuals produced on average two new infections, while for each two non-removed EVD-infected corpses a new infection occurs. Fast removal of EVD-infected corpses significantly reduces the attack rate per se. However, when combined to effective quarantine, fast removal of EVD-infected corpses substantially reduces the minimum quarantine capacity needed to eradicate EVD.

2.4.3 *The Impact of the Intervention Time on the Control of EVD*

Due to the lack of appropriate preparedness and capacity, local health care systems were fast overwhelmed during the West African EVD epidemic. In few weeks international aid became critical on boosting local health services to the point it was possible fight EVD. The epidemic quickly spread across the West Africa region, and in consequence, the time it took international community to reinforce local response against Ebola became critical, particularly after the implementation of *cordons sanitaires*. Calls for international aid were officially done after the virus reached highly dense populated cities, by the end of June 2014 Médecins Sans Frontières (MSF) declared the Ebola outbreak out of control, while until August 2014 the WHO declared it an international threat (UN, 2018).

Previous results studied the impact of quarantine implementation by assuming the control intervention is effective since the beginning of the epidemic. In this section, the impact of applying delayed quarantine programs as a control measure against an West African like EVD epidemic is studied. Numerical explorations focus on the effect of delayed quarantine implementation on the final number of EVD-infected individuals. In the explored scenar-

ios, the proportion of diagnosed individuals taking to quarantine is assumed constant over time, and quarantined individuals are assumed to be effectively isolated, $(l = 0)$.

Figure 2.11 shows the epidemic evolution when quarantine programs diagnosing 60%, 50%, 30% and none pre-symptomatic individuals are implemented 75 days after the index case. Particularly, it is shown that detecting and quarantining at least 60% of pre-symptomatic individuals produce a monotonic decreasing of the prevalence.
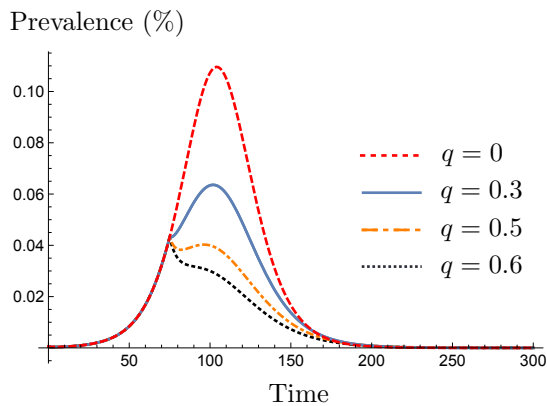
Figure 2.11: Effects of quarantine 60%, 50% 30% and no quarantine on the EVD prevalence, after 75 days of the index cases.
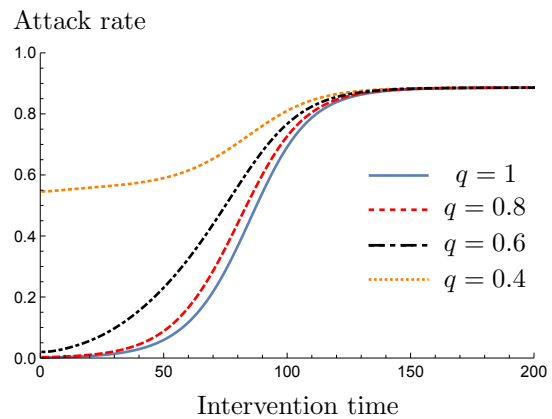
Figure 2.12: The effect of quarantine implementation time on the attack rate.

It is clear that control efforts' impact is strongly dependent on the implementation time. Figure 2.12, shows that late implementation of a massive and highly effective quarantine program diagnosing pre-symptomatic individuals, produces similar effects on the attack rate than early implementation of a smaller quarantine program. Thus, highlighting the importance of a fast response at local levels.

2.5   Discussion

Reverse Transcription Polymerase Chain Reaction (RT-PCR) technology offers new perspectives on the control strategies available against EVD, by early detecting EVD-infected individuals in a period of up to three days before symptoms onset. Results showed

that quarantine programs targeting pre-symptomatic individuals can eradicate an ongoing EVD outbreak provided high enough scope and a substantial reduction of quarantined individuals contagiousness. According to the presented model, high quarantine capacity is required even when perfect isolation is accomplished (at least 60% of the infected population). This minimal quarantine capacity is highly sensitive to both, quarantine effectiveness and EVD-infected corpses burial period. Particularly, reducing secondary infections produced by contacts with EVD-infected corpses, substantially reduces the efforts required to reduce the basic reproductive number bellow one. Furthermore, the impact of delayed quarantine implementation dramatically reduces over time. Not surprising, the impact of delayed massive quarantine programs providing perfect isolation on the attack rate, is comparable to earlier implemented local quarantine programs.

The fragile health system of the affected regions were incapable to provide an adequate fast response during the 2014 West African Ebola outbreak. This, when combined to the reduced effects of delayed implementation of control strategies allowed the EVD epidemic to became a catastrophic event, and call to allocate collective liability on improving sanitary conditions in the West African EVD vulnerable regions. The simplicity of the used model naturally leads to an overestimation on the dynamics of the EVD epidemic. Structured population models by incorporating population's heterogeneity might help to disentangle the role of localized interventions on the control of EVD.

Chapter 3

THE LAGRANGIAN APPROACH

Mathematical models of infectious diseases envision transmission through "collisions" between susceptible and infected individuals. These collisions or *contacts* assumed (in the simplest case) random over the population, represent the building blocks behind the contagion process (Castillo-Chavez et al., 2016). The impossibility of clearly defining what a *successful contact* means in the context of epidemiology, precede the difficulty to appropriately measure individuals' interactions. For instance, it has been shown that the concept of contact strongly affects model results. The assumption of contact types, contacts frequency and duration of contacts, as well as mixing patterns, play important roles in modeling a contagion process (Mossong et al., 2008). The issue of homogeneity in epidemiology has been addressed, for example, through meta-population models or models with patchy landscapes, and network-based models (Arino and Van den Driessche, 2006; Sattenspiel and Dietz, 1995; Arino and Van Den Driessche, 2003; Van den Driessche, 2008). Such models recognize the importance of a disease transmission dependent on the environment and individuals' activity varying across patches with different characteristics. Furthermore, by labeling individuals according to their place of residency, it is possible to track them across different regions at all times through the corresponding traveling rates.

Metapopulation models as tractable mathematical tools aimed to incorporate population's heterogeneity, usually require a large number of parameters in order to perform simulations. For instance in modeling the spread of Measles in the 1984 epidemic in Dominica (Sattenspiel and Dietz, 1995). The model used differentiated traveling rates between infants, school-age children and adults, thus becoming highly complex and requiring a lot of data to simulate. Recognizing the value of mathematical models as analytic tools from

23

which qualitative insights can be obtained is important. In this regard, simple models or models accounting for measurable parameters becomes paramount in order to couple mathematical modeling to data obtained from experimental works.

The Lagrangian perspective stresses this modeling principle by conceiving the infectious process as the result of individuals being exposed to different infection risks while sojourning in different environments (patches). A patch is conceived as any location where individuals' interactions can occur, and under the Lagrangian approach, it is endowed with a specific "transmission risk", β_i. This parameter collects patch specific attributes like social and economic conditions, health care access, among others. In this framework, the infection risk is an intrinsic property of the environment and independent of the population group. Individuals experience different risks of infection as they move across different environments, i.e. the risk of infection is seen as a function of the *residency time* spent in a given environment, or as a function of the proportion of contacts occurred (Bichara et al., 2015; Bichara and Castillo-Chavez, 2016; Castillo-Chavez et al., 2016, 2003). The Lagrangian perspective represents a simple, yet powerful way to build mathematical models including heterogeneity. Lagrangian approaches have been used, for instance, to study vector-borne diseases (Iggidr et al., 2016; Wesolowski et al., 2012). However, the framework used by researchers ignores the effect of mobility on the patch-specific population size at time t, that is, the patch population is composed by local individuals for all t. The Lagrangian framework through residency times used in the present work incorporates the concept of *effective population*. This is, the expected population in a given patch at time t, is composed by residents and visitant individuals, and ultimately weighted by the average activity level of these populations in each patch. Specifically, by letting N_i denote the predispersal (on isolation) Patch i population, the *effective population* size in Patch i at time t is given by $\sum_{j=1}^{n} p_{ji} N_j$. Furthermore, individuals' activity is monitored via a residency matrix $\mathbb{P} = (p_{ij})_{1 \le i, j \le n}$, where p_{ij} stands for Patch i residents' average proportion of time

spent in Patch j, per unit time, and $\sum_{j=1}^{n} p_{ij} = 1$ (Bichara et al., 2015; Castillo-Chavez et al., 2016; Bichara and Castillo-Chavez, 2016). In general, residency times are not constant over time and across populations groups. For example, the time an individual spends in different environments can be the result of the social behavior exhibited when facing an epidemic, in this scenario residency times might be a function of the proportion of the infectious population sojourning in each patch at time t. Hosts' response to illness has also been addressed through the Lagrangian approach via residence times. Under this scenario, the time an individual spend in a given environment varies according to the individual's epidemiological status (Bichara and Iggidr, 2017).

In the Lagrangian perspective, the total risk of infection perceived by a susceptible individual per unit time, is the sum of all the (in general different) infection risks experienced by such individual while sojourning on different environments. Individual's exposure to patch-specific risks is weighted by their corresponding activity level on each environment (residency time or proportion of contacts). This is, the classical force of infection term $\beta S \frac{I}{N}$ under the Lagrangian framework through residence times reads as follows

$$S_i \sum_{j=1}^{n} \beta_j p_{ij} \frac{\sum_{k=1}^{n} p_{kj} I_k}{\sum_{k=1}^{n} p_{kj} N_k} \tag{3.1}$$

where β_j stands for the Patch j risk of infection, p_{ij} is the average proportion of time Patch i residents spend in Patch j, and the infectious proportion of the population sojourning in Patch j is denoted by $\frac{\sum_{k=1}^{n} p_{kj} I_k}{\sum_{k=1}^{n} p_{kj} N_k}$. In summary, the Lagrangian approach incorporates heterogeneity by weighting individuals' activity levels (through proportion of contacts spent or the proportion of time sojourning in each environment) exhibited across environments which have different infection risks. The value of the Lagrangian approach through residency times resides on the parameter's clear definitions, which in turn allows for experimental assessment. For instance, the patch-specific infection risk can be experimentally measured as it is conceived as an intrinsic patch property. This increases the value of

25

mathematical models based on this framework, since the parameters used are potentially measurable. Previous work using the Lagrangian approach through residency times explored the effects of mobility in the context of Ebola, Tuberculosis and Zika (Espinoza et al., 2016; Moreno et al., 2017a,b). By using a simple two patch landscape, the impact of host-movement on the local and global transmission dynamics on neighboring regions having highly distinct infection risks is assessed. In the study of Ebola, the *cordons sanitaires* effectiveness was assessed by studying traveling ban in a two patch system consisting of equally dense populations.

Broader use of this framework can intuitively be constructed, for instance in ecology, in the problem of patch selection, incorporation of residency times would be a natural extension. Furthermore, the conception of patch as a geographical environment can also easily be generalized to a broader concept. For example, any system allowing for diverse "strategies" can be studied by thinking about these strategies as patches, while the "residency time" can be seen as the proportion of time a particular strategy is used, or as the weight a particular strategy has on the final output.

Chapter 4

CONSEQUENCES OF SHORT TERM MOBILITY ON THE WEST AFRICAN EBOLA OUTBREAK

4.1 Introduction

The largest Ebola Virus Disease (EVD) epidemic documented in history started on December 2013 in the West African region. The Ebola virus (EBOV), formerly designated Zaire ebolavirus and the most dangerous of the *Ebolavirus* genus, was identified as the culprit. Few days after the outbreak started in the village of Meliandou, Guéckédou Prefecture, in Guinea, secondary cases were also detected in the neighboring countries of Sierra Leone and Liberia. The epidemic quickly spread in the triple border of these countries, a region where high commercial transit considerably increased the likelihood of EVD international dissemination (Gomes et al., 2014).

In response against a rapidly evolving EVD otubreak, on August 1st, 2014 governments decided to implement a *cordons sanitaires*, a controversial old tactic used to stop the spread of an epidemic and not seen in centuries. The control strategy consisted on imposing traveling bans around the region containing the majority of the known cases. Individuals inside the cordoned area were banned from traveling outside, and borders were aggressively monitored by making use of military force (Agence France-Presse, 2018). Although the *cordons sanitaires* are aimed to avoid potential secondary cases produced outside the cordoned area, individuals within suffered from scarcity, lack of medical services and crowding, conditions potentially leading the affected population to experience an elevated risk of EVD infection (Amesh Adalja, 2018; R. K. Hoffmann et.al, 2018; Towers et al., 2014).

27

Many factors jointly acted to produce the catastrophic 2014 West African epidemic. Fragile local health infrastructure, and a population being exposed by first time to EVD, with a high devotion to unsafe traditional practices, affected the massive control efforts implementation and effectiveness (Matua et al., 2015; CDC, 2018c). Moreover, the commercial importance of the affected region exposed a large mobile population to EVD infection, these individuals traveled across regions absent of disease reigniting EVD transmission chains and as consequence promoting a generalized risk of infection across affected regions (WHO, 2018). The effectiveness of the *cordons sanitaires* strategy implemented during the West African outbreak has been previously analyzed by using a two patch model with differential risk (Espinoza et al., 2016). Authors showed that travel ban across neighboring regions having highly distinct sanitary conditions not always minimize the total EVD burden. Their results suggest the existence of mobility levels producing total EVD burden levels bellow the *cordons sanitaires* scenario.

In this chapter, a two-patch model coupled by tracking individual's residency times across patches, is used to study the dynamics of EVD on heterogeneous risk environments in the presence of mobility. By tracking individuals' place of residency and the proportion of time spent in each patch, the mobility conditions producing beneficial effects on the EVD control are assessed. It is assumed that one of the patches exhibits similar conditions to those seen within the cordoned area during the West African EVD epidemic, while the second patch is assumed to offer better sanitary conditions and a low infection risk. While sojourning in the cordoned patch ("high-risk" patch), individuals are assumed to experience a high risk of EVD infection, in counterpart, during the time spent outside the cordoned region ("low-risk" patch), individuals are assumed to experience a minimal EVD infection risk. Results suggest that allowing individuals from the cordoned region to spend time in the safer region can have beneficial or detrimental effects, depending on the mobility levels. While "low" mobility levels tend to produce a detrimental effect by increasing the

overall attack rate, "intermediate" and "high" mobility levels tend to be beneficial, reducing the overall attack rate. Furthermore, "high" mobility levels can mathematically control the EVD epidemic, provided a "safe enough" neighboring environment. Two mobility thresholds are identified, the *cordons sanitaires* threshold and the EVD control threshold, and their dynamics are assessed for various population's density ratios and patch-specific risks of infection.

The rest of the chapter is organized as follows, in Section 4.2, a single patch model describing EVD progression (in absence of control measures) among a population is derived. The single patch model's basic reproductive number and the final epidemic relation are computed. Section 4.3 is devoted to derive the two patch model with patch specific risks of infections in terms of residency times. Within Section 4.4 the analysis of the EVD dynamics on heterogeneous risk environments is presented, more precisely, the global basic reproductive number, the patch-specific basic reproductive and the global final epidemic size relation in the presence of mobility are computed. Section 4.5 contains the main results derived via numerical explorations. In Section 4.6, the final conclusions and a short discussion on the results implications are stated.

4.2   Model Derivation

The population of interest is structured by individual's epidemiological states: Susceptible (S), Latent (E), Infected (I), EVD-infected corpses (D) and, Removed EVD-infected corpses and Recovered individuals (R). The total population, including EVD-infected corpses is then, $N = S + E + I + D + R$. Susceptible individuals move to the infected compartment at rate $\beta \left(\frac{I + \varepsilon D}{N} \right)$ through "effective" contacts with either infected individuals (I) or EVD-infected corpses (D). Infected individuals spend on average $\frac{1}{\kappa}$ days on latency state, without being infectious. After the latency period, individuals become infectious (I) on average during $\frac{1}{\gamma}$ days, after which, individuals either recover with probability $(1 - f_d)$

29

or die with probability f_d. EVD-infected corpses (D) subpopulation is assumed to increase at rate $f_d\gamma$, and reduced through properly burial on average after $\frac{1}{\nu}$ days. Due to have the highest viral load, EVD-infected corpses are assumed to be more infectious than infected individuals (I), $\varepsilon > 1$. Figure 4.1 shows the EVD contagion process
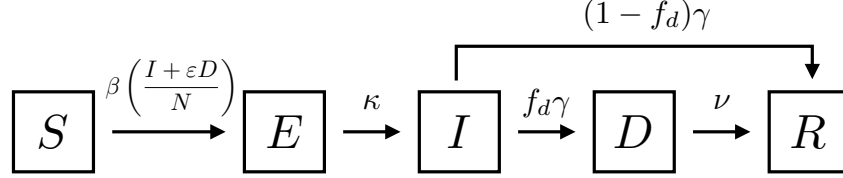
Figure 4.1: SEIDR model for Ebola Virus Outbreak

while system (4.1), mathematically describes population transitions through the EVD disease states

$$
\begin{cases}
N = S + E + I + D + R \\
\dot{S} = -\beta S \left(\frac{I + \varepsilon D}{N} \right) \\
\dot{E} = \beta S \left(\frac{I + \varepsilon D}{N} \right) - \kappa \\
\dot{I} = (1 - q)\kappa E - \gamma I \\
\dot{D} = f_d \gamma I - \nu D \\
\dot{R} = (1 - f_d)\gamma I + \nu D
\end{cases}
\tag{4.1}
$$

and Table 4.1 collects the parameter descriptions and values used in simulations

Table 4.1: Parameters of the single patch EVD model.

Parameter	Description	Base model values	
β	Per susceptible infection rate	0.287	(Althaus, 2014)
γ	Rate at which an infected recovers or dies	1/7	(Team, 2014)
κ	Per-capita progression rate to latent detectable stage	1/7	(Legrand et al., 2007)
ν	Per-capita body disposal rate	1/2	(Legrand et al., 2007)
f_d	Proportion of infected who die due to infection	0.7	(Team, 2014)
ε	Scale: Ebola infectiousness of EVD-infected corpses	> 1	(Li et al., 2016)

The population in (4.1) is constant and $\Omega = \{(S,E,I,R) \in \mathscr{R}_+^4 | S+E+I+R \leq N\}$ is a compact positively invariant set, hence solutions of (4.1) behave as biologically expected. By using the next generation approach, with disease compartments E, I, D the associated basic reproductive number is computed (Diekmann et al., 1990; van den Driessche and Watmough, 2002),

$$\mathscr{R}_0 = \beta \left(\frac{1}{\gamma} + \frac{\varepsilon f_d}{v} \right). \tag{4.2}$$

The basic reproductive number of system (4.1) captures the average number of secondary infections produced by a typical infectious individual during their infectious period $\left(\frac{\beta}{\gamma} \right)$, and the secondary cases generated by a single EVD-infected corpse, during its disposal period $\left(\frac{\varepsilon \beta f_d}{v} \right)$, in a totally susceptible population. The final size of the epidemic, in terms of the final proportion of infected population (attack rate) is expressed as follows

$$\log \frac{N}{S^\infty} = \mathscr{R}_0 \left(1 - \frac{S^\infty}{N} \right). \tag{4.3}$$

Equation (4.3) is called the *final size relation*, and it gives a relationship between the basic reproductive number and the size of the epidemic (Brauer et al., 2001).

4.3 Ebola Dynamics on Heterogeneous Risk Environments

Structured population models have been used to, for example, study the impact of a particular groups in a population or design targeted disease surveillance strategies. This approach allows to assess the accuracy of local specific characteristics as indicators of the large scale behavior of, for instance, the spread of an epidemic (Keeling, 1999; Eubank et al., 2004; Stroud et al., 2007). However, for structured models to prove valuable in practical epidemiological scenarios, they must require both specific and measurable parameters allowing for experimental design in order to obtain specific data for model calibration (Keeling, 1999; Castillo-Chavez et al., 2016). Frameworks implementing the Lagrangian perspective seems to be ad-hoc to this task, by tracking individuals according to their place

of residency at all times, the population's specific impact on the overall disease dynamics can be assessed (Castillo-Chavez et al., 2003; Bichara et al., 2015).

This work uses the Lagrangian approach through *residency times* to track individuals' activity on a two patch setting, i.e the proposed model assess the average proportion of time individuals' spent in each patch through the residency times matrix $\mathbb{P} = (p_{ij})$, $i, j \in \{1,2\}$, where $p_{ij} \geq 0$ are constant over time (Bichara et al., 2015; Castillo-Chavez et al., 2016). In this way, homogeneity is broken at the patch scale, while individuals' behavior within patches is assumed homogeneous. The community of interest is assumed to be composed by two adjacent regions facing distinct levels of EVD infection. Differences on risks of infection captures in a single parameter specific patch's attributes as economy levels, education access, healthcare access, cultural practices, etc.

The new cases of infection per unit time are modeled by incorporating the *effective density* of individuals sojourning in each patch, i.e. the expected amount of residents and visitants sojourning in Patch i at time t. By following the previous reasoning, the new infections within Patch j residents are given by

$$\varphi(j) = \underbrace{\beta_i}_{\text{Patch } i \text{ infection risk}} \underbrace{p_{ji}S_j}_{\text{Expected Patch } j \text{ susceptible pop. in Patch } i} \underbrace{\frac{p_{ii}I_i + p_{ji}I_j}{p_{ii}N_i + p_{ji}N_j}}_{\text{Proportion of infected pop. in Patch } i}$$

(4.4)

$$+ \underbrace{\beta_j}_{\text{Patch } j \text{ infection risk}} \underbrace{p_{jj}S_j}_{\text{Expected Patch } j \text{ susceptible pop. in Patch } j} \underbrace{\frac{p_{ij}I_i + p_{jj}I_j}{p_{ij}N_i + p_{ji}N_j}}_{\text{Proportion of infected pop. in Patch } j}$$

(4.5)

this is, Patch j residents can get infected at their patch of residency (with risk of infection β_j) and while sojourning in Patch i (with risk of infection β_i). Since times of residency holds $p_{ii} + p_{ij} = 1$, in the proposed two patch system, t_i is used to denote the Patch i residents' average proportion of time in Patch j, while $1 - t_i$ denotes the average proportion

of time Patch i residents' spend in their own patch. Hence the expected proportion of infected population sojourning in Patch i at time t is expressed as

$$\frac{(1-t_i)I_i+t_jI_j}{(1-t_i)N_i+t_jN_j} \tag{4.6}$$

Finally, the proposed model assumes that EVD-infected corpses are not transported across patches, and secondary infections produced by EVD-infected corpses occurs over the local population. In other words, burial events are assumed to be practiced by resident local individuals. Thus, by following the construction of model (4.1), the dynamics of EVD in a two patch landscape, with distinct risk of infection is described by the following system of differential equations

$$
\begin{cases}
N_i = S_i + E_i + I_i + D_i + R_i \\[2mm]
\dot{S}_i = -(1-t_i)\beta_i S_i\left(\frac{(1-t_i)I_i+t_jI_j}{(1-t_i)N_i+t_jN_j} + \frac{\varepsilon D_i}{N_i}\right) - t_i\beta_j S_i\left(\frac{t_iI_i+(1-t_j)I_j}{t_iN_i+(1-t_j)N_j}\right) \\[2mm]
\dot{E}_i = (1-t_i)\beta_i S_i\left(\frac{(1-t_i)I_i+t_jI_j}{(1-t_i)N_i+t_jN_j} + \frac{\varepsilon D_i}{N_i}\right) + t_i\beta_j S_i\left(\frac{t_iI_i+(1-t_j)I_j}{t_iN_i+(1-t_j)N_j}\right) - \kappa E_i \\[2mm]
\dot{I}_i = \kappa E_i - \gamma I_i \\[2mm]
\dot{D}_i = f_{\mathrm{d}}\gamma I_i - v_i D_i \\[2mm]
\dot{R}_i = (1-f_{\mathrm{d}})\gamma I_i + v_i D_i
\end{cases}
\tag{4.7}
$$

where $i,j \in \{1,2\}$ and $i \neq j$.

4.4   Model Analysis

4.4.1   EVD Basic Reproductive Number on Heterogeneous Risk Environments

System's (4.7) control and basic reproduction numbers are computed by following the next generation approach (Diekmann et al., 1990; van den Driessche and Watmough, 2002). Consider the infectious compartments E_1, I_1, D_1, E_2, I_2 and D_2, evaluating at the Disease

Free Equilibrium (DFE), leads to $S_1(0) = N_1$ and $S_2(0) = N_2$. Then

$$\mathscr{F} = \begin{pmatrix} (1-t_1)\beta_1 S_1 \left(\frac{(1-t_1)I_1 + t_2 I_2}{(1-t_1)N_1 + t_2 N_2} + \frac{\varepsilon D_1}{N_1} \right) + t_1 \beta_2 S_1 \left(\frac{t_1 I_1 + (1-t_2)I_2}{t_1 N_1 + (1-t_2)N_2} \right) \\ 0 \\ 0 \\ t_2 \beta_1 S_2 \left(\frac{(1-t_1)I_1 + t_2 I_2}{(1-t_1)N_1 + t_2 N_2} \right) + (1-t_2)\beta_2 S_2 \left(\frac{t_1 I_1 + (1-t_2)I_2}{t_1 N_1 + (1-t_2)N_2} + \frac{\varepsilon D_2}{N_2} \right) \\ 0 \\ 0 \end{pmatrix}$$

and

$$\mathscr{V} = \begin{pmatrix} \kappa E_1 \\ -\kappa E_1 + \gamma I_1 \\ -f_d \gamma I_1 + v_1 D_1 \\ \kappa E_2 \\ -\kappa E_2 + \gamma I_2 \\ -f_d \gamma I_2 + v_2 D_2 \end{pmatrix},$$

evaluated at the DFE, $S_1^* = N_1$ and $S_2^* = N_2$. Hence

$$F = \left(\begin{array}{c|c} J_1 & K_1 \\ \hline K_2 & J_2 \end{array} \right)$$

where

$$J_i = \begin{pmatrix} 0 & M_i & (1-t_i)\varepsilon\beta_i \\ 0 & 0 & 0 \\ 0 & 0 & 0 \end{pmatrix}, \qquad K_i = \begin{pmatrix} 0 & C_i & 0 \\ 0 & 0 & 0 \\ 0 & 0 & 0 \end{pmatrix},$$

and

$$M_i = \frac{N_i(1-t_i)^2\beta_i}{(1-t_i)N_i + t_j N_j} + \frac{t_i^2 N_i \beta_j}{t_i N_i + (1-t_j)N_j}, \quad C_i = \frac{(1-t_i)N_i t_j \beta_i}{(1-t_i)N_i + t_j N_j} + \frac{t_i(1-t_j)N_i \beta_j}{t_i N_i + (1-t_j)N_j},$$

and

$$V = \begin{pmatrix} \kappa & 0 & 0 & 0 & 0 & 0 \\ -\kappa & \gamma & 0 & 0 & 0 & 0 \\ 0 & -f_d\gamma & v_1 & 0 & 0 & 0 \\ 0 & 0 & 0 & \kappa & 0 & 0 \\ 0 & 0 & 0 & -\kappa & \gamma & 0 \\ 0 & 0 & 0 & 0 & -f_d\gamma & v_2 \end{pmatrix}.$$

The basic reproduction number of model (4.7), in the presence of mobility, is given by the spectral radius of the next generation matrix, $\mathscr{R}_0(t_1, t_2) = \rho(-FV^{-1})$. Note that the basic reproductive number is a function of the patch-specific mobility and risk levels ($\mathbb{P}$ and β_i respectively), as well as patch-specific densities (N_i).

4.4.2   EVD Final Epidemic Size on Heterogeneous Risk Environments

By using the notation $\hat{f}(t) = \int_0^\infty f(s)ds$ and $f^\infty = \lim_{t\to\infty} f(t)$, it is possible to find the Patch-specific final epidemic size, as function of times of residency. By assuming $S_i(0) = N_i$, $E_{1i}(0) = E_{2i}(0) = I_i(0) = Q_i(0) = D_i(0) = 0$, and by adding the first two equations $\dot{S}_i + \dot{E}_{1i} = -\kappa_1 \hat{E}_{1i}$, then $E_{1i}^\infty = 0$. Following the same reasoning $E_{2i}^\infty = I_i^\infty = Q_i^\infty = D_i^\infty = 0$. From the first two equations $\hat{E}_{1i} = \frac{N_i - S_i^\infty}{\kappa_1}$, and similar reasoning leads to $\hat{E}_{2i} = \frac{N_i - S_i^\infty}{\kappa_2}$, $\hat{I}_i = (N_i - S_i^\infty)\frac{(1-q_i)}{\gamma}$, $\hat{Q}_i = (N_i - S_i^\infty)\frac{q_i}{\gamma}$, $\hat{D}_i = (N_i - S_i^\infty)\frac{(1-q_i)f_d v_i}{\gamma}$.

From model's (4.7) first equation, the secondary infections among the Patch i population, produced by Patch i and Patch j individuals are given by

$$\log\left(\frac{N_1}{S_1^\infty}\right) = (N_1 - S_1^\infty)\left((1-t_1)\beta_1\left(\frac{\frac{(1-t_1)}{\gamma}}{(1-t_1)N_1+t_2N_2} + \frac{\frac{\varepsilon f_d}{v_1}}{N_1}\right) + t_1\beta_2\frac{\frac{t_1}{\gamma}}{t_1N_1+(1-t_2)N_2}\right)$$

$$+ (N_2 - S_2^\infty)\left((1-t_1)\beta_1\frac{\frac{t_2}{\gamma}}{(1-t_1)N_1+t_2N_2} + t_1\beta_2\frac{\frac{(1-t_2)}{\gamma}}{t_1N_1+(1-t_2)N_2}\right)$$

$$\log\left(\frac{N_2}{S_2^\infty}\right) = (N_1 - S_1^\infty)\left((1-t_2)\beta_2\frac{\frac{t_1}{\gamma}}{t_1N_1+(1-t_2)N_2} + t_2\beta_1\frac{\frac{(1-t_1)}{\gamma}}{(1-t_1)N_1+t_2N_2}\right)$$

$$+ (N_2 - S_2^\infty)\left((1-t_2)\beta_2\left(\frac{\frac{(1-t_2)}{\gamma}}{t_1N_1+(1-t_2)N_2} + \frac{\frac{\varepsilon f_d}{v_2}}{N_2}\right)\right.$$

$$\left. + t_2\beta_1\frac{\frac{t_2}{\gamma}}{(1-t_1)N_1+t_2N_2}\right)$$

which is expressed in vector form as

$$\begin{bmatrix} \log\left(\dfrac{N_1}{S_1^\infty}\right) \\ \log\left(\dfrac{N_2}{S_2^\infty}\right) \end{bmatrix} = \begin{bmatrix} B_{11} & B_{12} \\ B_{21} & B_{22} \end{bmatrix} \begin{bmatrix} 1 - \dfrac{S_1^\infty}{N_1} \\ 1 - \dfrac{S_2^\infty}{N_2} \end{bmatrix} \tag{4.8}$$

where

$$B_{11} = \left((1-t_1)\beta_1 \left(\frac{\frac{(1-t_1)}{\gamma}}{(1-t_1)N_1 + t_2 N_2} + \frac{\frac{\varepsilon f_d}{v_1}}{N_1} \right) + t_1 \beta_2 \frac{\frac{t_1}{\gamma}}{t_1 N_1 + (1-t_2)N_2} \right) N_1,$$

$$B_{12} = \left((1-t_1)\beta_1 \frac{\frac{t_2}{\gamma}}{(1-t_1)N_1 + t_2 N_2} + t_1 \beta_2 \frac{\frac{(1-t_2)}{\gamma}}{t_1 N_1 + (1-t_2)N_2} \right) N_2,$$

$$B_{21} = \left((1-t_2)\beta_2 \frac{\frac{t_1}{\gamma}}{t_1 N_1 + (1-t_2)N_2} + t_2 \beta_1 \frac{\frac{(1-t_1)}{\gamma}}{(1-t_1)N_1 + t_2 N_2} \right) N_1$$

$$B_{22} = \left((1-t_2)\beta_2 \left(\frac{\frac{(1-t_2)}{\gamma}}{t_1 N_1 + (1-t_2)N_2} + \frac{\frac{\varepsilon f_d}{v_2}}{N_2} \right) + t_2 \beta_1 \frac{\frac{t_2}{\gamma}}{(1-t_1)N_1 + t_2 N_2} \right) N_2.$$

Model's (4.7) final size relation is denoted by the patch-specific final proportion of infected individuals (or attack rate)

$$\begin{bmatrix} 1 - \dfrac{S_1^\infty}{N_1} \\[2mm] 1 - \dfrac{S_2^\infty}{N_2} \end{bmatrix},$$

and the matrix B, capturing the secondary infections produced by Patch 1 and Patch 2 individuals in each environment. For instance, B_{12} accounts for the Patch 1 residents infected by Patch 2 inhabitants in both environments, while spending $1-t_1$ time in their patch of residency and having contact with an infected Patch 2 visitor individual at rate

$$(1-t_1)\beta_1 \frac{\frac{t_2}{\gamma}}{(1-t_1)N_1 + t_2 N_2}$$

and while visiting Patch 2 and being infected by Patch 2 inhabitants at rate

$$t_1 \beta_2 \frac{\frac{(1-t_2)}{\gamma}}{t_1 N_1 + (1-t_2)N_2}.$$

Furthermore, the eigenvalues of the matrix B on the final epidemic size are the same of the second generation matrix, then the global basic reproductive number is also the spectral

37

radius of B (Bichara et al., 2015). Under this framework the global reproductive number is a function of the mobility matrix ($\mathbb{P}$) and the patch specific basic reproductive numbers ($\mathscr{R}_{0i}$), defined in the absence of mobility ($t_1 = t_2 = 0$), so that, $\mathscr{R}_0 = f(\mathbb{P}, \mathscr{R}_{01}, \mathscr{R}_{02})$.

Let $s_i^\infty = \lim\limits_{t \to \infty} \dfrac{S_i(t)}{N_i}$, represent the proportion of the population remained susceptible at the end of the epidemic. Then, from equation (4.8)

$$s_1^\infty = \exp[-B_{11}(s_1^\infty - 1) - B_{12}(s_2^\infty - 1)],$$
$$s_2^\infty = \exp[-B_{21}(s_1^\infty - 1) - B_{22}(s_2^\infty - 1)].$$

which in terms of the total number of disease cases from Patch i over the course of the epidemic ($y_i = 1 - s_i^\infty$), takes the form

$$y_1 = 1 - \exp[-y_1 B_{11}]\exp[-y_2 B_{12}],$$
$$y_2 = 1 - \exp[-y_1 B_{21}]\exp[-y_2 B_{22}].$$
(4.9)

System's (4.9) solution (y_1^*, y_2^*), represents the patch-specific attack rates. Therefore, the total final epidemic size (φ) as a function of the patch-specific density, risk and mobility levels, is given by

$$\varphi(N_1, N_2, \mathscr{R}_{01}, \mathscr{R}_{02}, t_1, t_2) = N_1 y_1^* + N_2 y_2^*$$
(4.10)

4.4.3 The Patch-Specific Basic Reproductive Number in the Presence of Mobility

The patch-specific basic reproductive number in the absence of mobility incorporates the secondary infections produced among the resident population. In the presence of mobility, the Patch-specific basic reproductive number should accounts for the secondary infections produced among the resident and the visiting population, where the secondary infections generated can occur through contacts with locals or visitant infected individuals. The threshold condition for disease prevalence among the Patch i population, when individuals experience differential risk while moving across patches, spending on average p_{ij}

proportion of their time in Patch j, reads as follows

$$\mathscr{R}_0^i(\mathbb{P}) = \mathscr{R}_0^i \times \sum_{j=1}^n \left(\frac{\beta_j}{\beta_i}\right) p_{ij} \left(\frac{\left(p_{ij}\frac{b_i}{d_i}\right)}{\sum_{k=1}^n p_{kj}\frac{b_k}{d_k}}\right) \tag{4.11}$$

where β_i stands for the Patch i infection risk, p_{ij} is the average proportion of time individuals from Patch i spend in Patch j, $\mathscr{R}_0^i$ represents the Patch i basic reproductive number in the absence of mobility and $\frac{b_i}{d_i}$ is the Patch i population at equilibrium (Bichara et al., 2015). Initially the aforementioned condition was stated as the patch-specific basic reproductive number. However, the patch-specific basic reproductive number must be dependent uniquely on the local infection risk. Furthermore, model construction implies that the $\dot{S}_i$ equation captures the secondary infections produced among Patch i individuals across environments.

In this work, an expression accounting for the secondary infections produced in each environment is derived from the computation of the total final epidemic size relation expressed by equation (4.8), and particularly, by using the associated matrix B, which captures the secondary infections produced in each environment. Denoting $\varphi = \log\left(\frac{N_1}{S_1^\infty}\right) + \log\left(\frac{N_2}{S_2^\infty}\right)$, the total final size relation can be expressed in terms of the infections generated

in each environment as follows

$$\varphi = \underbrace{(N_1 - S_1^\infty)\left[(1-t_1)\beta_1\left(\frac{(1-t_1)/\gamma}{(1-t_1)N_1 + t_2N_2} + \frac{\varepsilon f_d/\nu_1}{N_1}\right) + (1-t_1)\beta_1\frac{t_2/\gamma}{(1-t_1)N_1 + t_2N_2}\right]}_{\text{Patch 1 residents infected in Patch 1}}$$

$$+ \underbrace{(N_2 - S_2^\infty)\left[t_2\beta_1\left(\frac{(1-t_1)/\gamma}{(1-t_1)N_1 + t_2N_2}\right) + t_2\beta_1\frac{t_2/\gamma}{(1-t_1)N_1 + t_2N_2}\right]}_{\text{Patch 2 residents infected in Patch 1}}$$

$$+ \underbrace{(N_1 - S_1^\infty)\left[t_1\beta_2\left(\frac{t_1/\gamma}{t_1N_1 + (1-t_2)N_2}\right) + t_1\beta_2\frac{(1-t_2)/\gamma}{t_1N_1 + (1-t_2)N_2}\right]}_{\text{Patch 1 residents infected in Patch 2}}$$

$$+ \underbrace{(N_2 - S_2^\infty)\left[\begin{array}{l}(1-t_2)\beta_2\left(\dfrac{t_1/\gamma}{t_1N_1 + (1-t_2)N_2}\right) \\[2mm] + (1-t_2)\beta_2\left(\dfrac{(1-t_2)/\gamma}{t_1N_1 + (1-t_2)N_2} + \dfrac{\varepsilon f_d/\nu_2}{N_2}\right)\end{array}\right]}_{\text{Patch 2 residents infected in Patch 2}}.$$

where all the secondary infections produced in Patch i (ρ_i) are given by

$$\rho_i = \frac{\beta_i}{(1-t_i)N_i + t_jN_j}\left[(1-t_i)N_i\left(\frac{1-t_i}{\gamma} + \frac{t_j}{\gamma} + \frac{\varepsilon f_d/\nu_i}{N_i}((1-t_i)N_i + t_jN_j)\right)\left(1 - \frac{S_i^\infty}{N_i}\right)\right.$$
$$\left. + t_jN_j\left(\frac{1-t_i}{\gamma} + \frac{t_j}{\gamma}\right)\left(1 - \frac{S_j^\infty}{N_j}\right)\right] \quad \text{for} \quad i,j \in \{1,2\}, \, i \neq j.$$

Finally, by ignoring the place of residency of infected individuals in Patch i the patch-specific basic reproductive numbers for model (4.1), in the presence of mobility, are expressed by

$$\mathscr{R}_{0i}(\mathbb{P}) = (1-t_i)\beta_i\left(\frac{1}{\gamma} + \frac{f_d\varepsilon}{\nu_i}\right) + t_j\beta_i\frac{1}{\gamma} \tag{4.12}$$
$$= (1-t_i)\mathscr{R}_{0i} + t_j\beta_i\frac{1}{\gamma}, \quad \text{for} \quad i,j \in \{1,2\}, \, i \neq j.$$

Equation (4.12), accounts for the secondary infections produced within Patch i, among local and visitant individuals, weighted by the corresponding residency time. More specifically, the average secondary infections produced among Patch i individuals while in Patch i,

is captured by the term $(1-t_1)\mathscr{R}_{01}$, and the average secondary infections produced among Patch j residents while in Patch i, is expressed by the term $t_j \beta_i \frac{1}{\gamma}$. The asymmetry exhibited in the patch-specific basic reproductive number is due to the model construction, the assumption that EVD-infected corpses are locally handled implies that secondary infections on the visiting population are generated only by infected individuals but not EVD-infected corpses. Moreover, note that $\mathscr{R}_{0i}(\mathbb{P})$ is independent of the population density, a property inherited by the so called "standard incidence" used in the construction of the model (Brauer et al., 2001). In a totally symmetric n patch model, i.e. where the resident and the visitant populations experience the same routes of infection, the patch-specific basic reproductive number is expected to accounts for all the secondary infections produced within Patch i, among individuals from each patch and weighted by the population's residency times in Patch i, this is

$$\mathscr{R}_{0i}(\mathbb{P}) = \mathscr{R}_{0i} \times \sum_{j=1}^{n} p_{ji}. \tag{4.13}$$

In the Lagrangian perspective through residence times, the patch-specific basic number number in the presence of mobility $\mathscr{R}_{0i}(\mathbb{P})$, is proportional to the patch basic reproductive number in the absence of mobility ($\mathscr{R}_{0i}$), where the cumulative residency time individuals from all patches spend in Patch i is the constant of proportionality.

Figure 4.2 shows the dynamics of the global $\mathscr{R}_0(\mathbb{P})$, and the patch patch-specific basic reproductive numbers $\mathscr{R}_{0i}(\mathbb{P})$, in the presence of one way mobility ($t_2 = 0$).
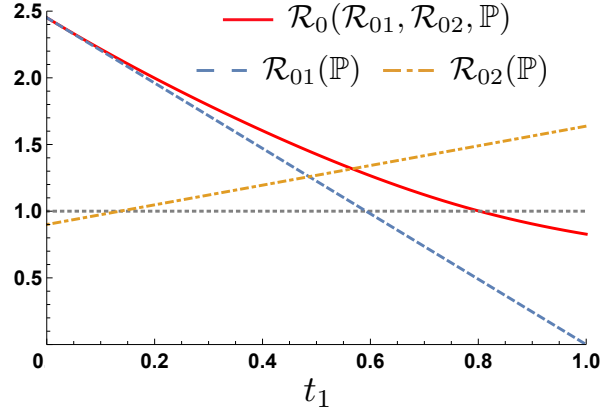
Figure 4.2: Global and patch-specific basic reproductive numbers in the presence of mobility.

In this section, a mathematical expression for the mobility required to reduce the total final epidemic size bellow the *cordons sanitaires* scenario is derived. Hereafter called the *cordons sanitaires* mobility threshold, the minimum mobility required to produce a beneficial effect can be numerically addressed by using equations (4.10) and (4.3). By the typical final size relation, the attack rate can be numerically computed by solving the equation $y = 1 - \exp[-y\mathscr{R}_0]$ (Brauer et al., 2001). Then, Ny^* stands for the final epidemic size in the absence of mobility. According to previous derivations, the overall final epidemic size in presence of mobility is denoted by (4.10), where y_i^* stands for the patch-specific attack rate in presence of dispersal. By assuming the high-risk patch (Patch 1) is cordoned, and that there is no traveling from the safer patch (Patch 2), the *cordons sanitaires* threshold is defined as the Patch 1 average proportion of time $(t_1 \neq 0)$ such that

$$y^* = \varphi(N_1, N_2, t_1) \tag{4.14}$$

4.5 Results

In this section the local and global effects of population dispersal on the global EVD dynamics is studied. On a two patch landscape, the effects of mobility across patches

with equal density ($N_1 = N_2 = 10,000$) is studied. In order to capture sanitary differences between patches, in the absence of mobility Patch 1 is assumed capable to sustain an epidemic, $\mathscr{R}_{01} > 1$), while Patch 2 is assumed incapable to do so, meaning that $\mathscr{R}_{02} < 1$. The presented model is calibrated to data from the West African EVD outbreak to get $\mathscr{R}_{01} = 2.45$, (Towers et al., 2014; Chowell and Nishiura, 2014; Althaus, 2014). Under the aforementioned setup the impact of mobility from the high and low risk patches on the final epidemic size is numerically explored. Particularly, the mobility conditions under which the *cordons sanitaires* strategy is effective or detrimental are explored. Moreover, the effects of population densities and risk disparities on the control of EVD through mobility are assessed.

4.5.1 The Impact of High-Risk Population Mobility

Intuitively, it makes sense to expect that spreading a disease through individuals moving to a region basically consisting of completely susceptible individuals, has the potential to increase the overall final epidemic size. However, if the affected population travels to a region having better sanitary conditions, a trade off between reducing secondary infections in the high-risk region, and increasing them in a more prepared area, will occurs. This is, although the resident population of the safe region is being infected by having contacts with visitant infected individuals, safer sanitary conditions locally reduce the strength of the epidemic.

Figure 4.3 shows the non-linear effects of allowing Patch 1 (high-risk) population spend a proportion of their daily time in the safer region, on the patch-specific and total final epidemic size. Individuals from the safer patch are assumed to avoid the high-risk region, then model (4.7) is calibrated to $t_2 = 0$. By taking the final epidemic size corresponding to the uncoupled scenario as baseline (dashed gray line), results suggest that low mobility levels increase the total final epidemic size ($t_1 < 0.5$), while "big enough" traveling levels

43

takes it down the *cordons sanitaires* scenario, ($t_1 > 0.5$). Moreover, results suggest that high levels of single direction mobility can also control an ongoing EVD outbreak, ($t_1 > 0.8$). This last observation reflects the sharp threshold condition of disease persistence in the overall system of the Lagrangian framework through residence times (Bichara et al., 2015).

This work focus on the aforementioned traveling thresholds, namely, the traveling required to reduce the total attack rate bellow the *cordons sanitaires* scenario (t_1^-), and the traveling needed to control an EVD outbreak in the whole system, (t_1^+). The first threshold denotes the mobility level producing a total attack rate equal to the *cordons sanitaires* scenario, while the second threshold represents the mobility at which the global basic reproductive number ($\mathscr{R}_0(\mathbb{P}, \mathscr{R}_{01}, \mathscr{R}_{02})$), hits one. Particularly, the t_1^- threshold captures the trade off between diminishing cases in Patch 1, while increasing infected individuals in Patch 2.
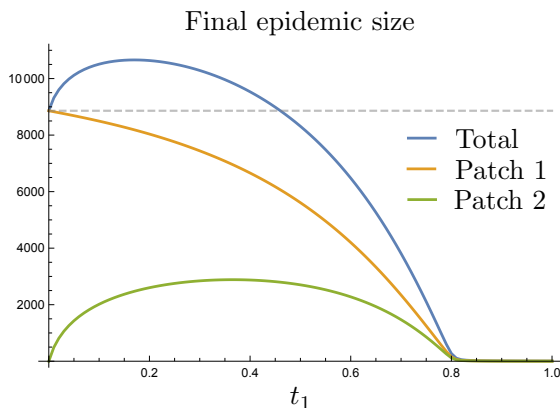
Figure 4.3: Patch specific and total final epidemic size under one way mobility ($t_2 = 0$).
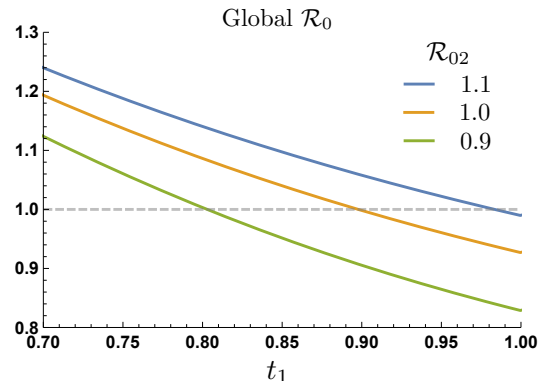
Figure 4.4: Global $\mathscr{R}_0$ for different Patch 2 risk scenarios, $t_2 = 0$.

Figure 4.4 shows that the existence of a threshold after which unidirectional mobility can control an EVD outbreak, is tied to the Patch 2 risk of infection. For instance, the scenario exhibited in Figure 4.3, corresponds to $\mathscr{R}_{01} = 2.45$ and $\mathscr{R}_{02} = 0.9$, where mobility above $t_1 = 0.8$, produces a global $\mathscr{R}_0$ less than one, thus leading the final epidemic size to almost zero. It is worth to mention that the curves in Figure 4.4 do not converge to $\mathscr{R}_{02}$

at the extreme value $t_1 = 1$, this is because model (4.7) is asymmetric due to the local management of EVD-infected corpses.

Figure 4.5 shows that the t_1^- and t_1^+ thresholds are highly sensitive to the Patch 2 risk of infection. This is, both thresholds are functions of the Patch 2 risk of infection, $t_1^- = t_1^-(\mathscr{R}_{02})$ and $t_1^+ = t_1^+(\mathscr{R}_{02})$. Hence, reduction of the Patch 2 infection risk ameliorates EVD secondary infections and relaxes mobility conditions required to appropriately manage an epidemic on the overall system.
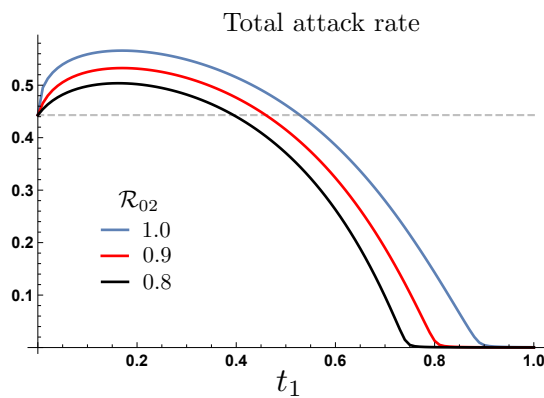
Figure 4.5: Total attack rate for different Patch 2 risk levels, under one way mobility.
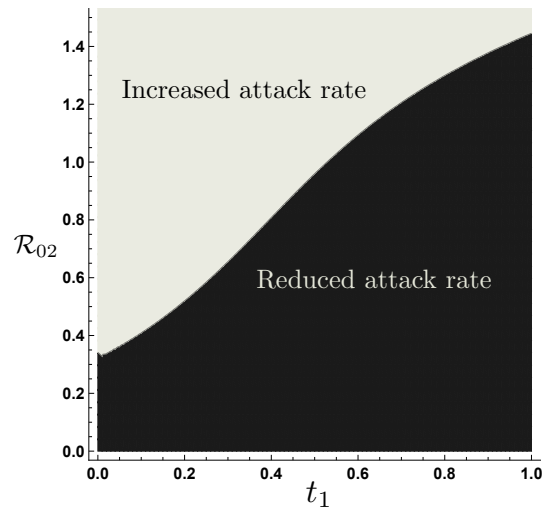
Figure 4.6: Traveling time reduces or increases the total attack rate, as function of the Patch 2 risk of infection.

Figure 4.6 shows the impact of Patch 2 sanitary conditions and mobility from the high-risk region, on the effectiveness of the *cordons sanitaires* strategy. The traveling and risk conditions for which the total attack rate increases or decreases, characterize three scenarios for the *cordons sanitares* effectiveness

- For a "highly safe" Patch 2, ($\mathscr{R}_{02} < 0.35$), all mobility levels from the high-risk region are beneficial. This is, the total attack rate monotonically decreases as t_1 increases. Hence, implementation of the *cordons sanitares* under this scenario is the worst decision.

- Given an "intermediately safe" Patch 2, ($0.35 < \mathscr{R}_{02} < 1.45$), depending on the mobility levels, the total attack rate increases or decreases. Therefore, under these scenarios, the *cordons sanitaires* strategy is effective provided specific mobility levels required to reduce the total attack rate are not attainable. In other words, whenever mobility from the high-risk patch is lower than $t_1^- (\mathscr{R}_{02})$, the *cordons sanitaires* control measure is not recommended.

- For an "unsafe" Patch 2 ($\mathscr{R}_{02} > 1.45$), all mobility levels increase the total attack rate. In these scenarios, even when Patch 2 is considerably safer than Patch 1, the reduced risk of infection is not enough to produce an overall benefit reducing the total number of infections. Therefore, in these scenarios the implementation of *cordons sanitaires* is an effective control strategy.

According to the aforementioned results, the *cordons sanitaires* scenario do not always minimize the overall number of infected individuals, and under specific risk conditions it may or may not be effective. Its impact on the total attack rate is rather determined by the Patch 2 risk of infection. Moreover, its implementation has to be evaluated taking in account the specific attributes of the community of interest. Particularly, characterization of the health care system in the safer patch is important in order to evaluate control measures in the form of a traveling ban.

Figure 4.7 shows the level curve $\mathscr{R}_0(t_1, \mathscr{R}_{02}) = 1$ in the plane $(t_1, \mathscr{R}_{02})$. The mobility and risk conditions where an EVD outbreak can and cannot be sustained are distinguished.
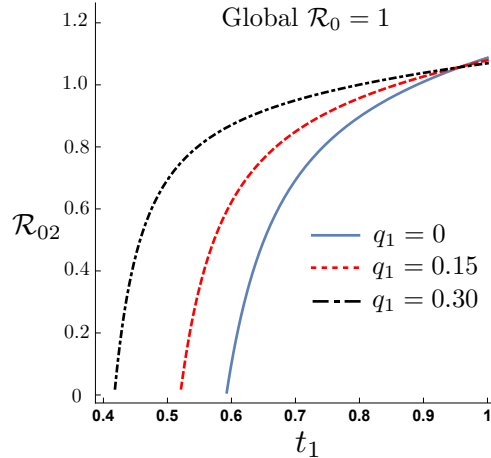
Figure 4.7: Mobility from high risk patch can eradicate an EVD outbreak, $(N_1 = N_2)$

According to simulations, mobility can eradicate an EVD epidemic given the low-risk patch is "safe" enough. For the model calibrated to data of the 2014 West African Ebola outbreak, high mobility can control an EVD outbreak even when $\mathscr{R}_{02}$ is slightly greater than one. However, even under the extreme scenario of a completely safe Patch 2 ($\mathscr{R}_{02} = 0$), controlling an EVD outbreak will require high-risk patch residents to spend at least around 60% of their time outside the highly affected region.

Due to the extraordinary efforts that substantial improvement of sanitary conditions in the high risk region would demand, alternative control strategies leading to the eventual EVD control become meaningful. Previous results show that traveling management has the potential, as an alternative control strategy, to minimize the total attack rate. Nonetheless, it is important to notice that such goal would require massive mobility. More important yet, it should be noticed that on managing mobility as a control strategy, a fraction of the safer patch residents is expected to be infected. Thus, an effective mobility strategy aimed to minimize the total number of final infected individuals, requires a safer patch willing to receive part of the disease morbidity. Reduction of the EVD total attack rate through mobility implies the spread of the outbreak to an environment free of the disease. Increasing the local disease cost in terms of secondary cases in the safe patch, but decreasing the

overall disease burden. Finally, mobility management might be a counter intuitive control strategy, and if not appropriately used it has the potential to produce adverse effects.

4.5.2   The Impact of Low-Risk Population Mobility

The West African EVD outbreak taught us that sustainability of regions highly vulnerable to EVD infection and, its dependence on neighboring regions is a critical issue on the EVD control. Food transportation, health care services, commerce, etc., are critical factors for a population to persist. Some of these, necessarily require traveling from and to high-risk of infection zones, potentially exposing neighboring susceptible population to EVD infection. In order to analyze the impact of traveling from the low-risk of infection zone on the EVD dynamics, the effects of allowing two ways traveling on system (5.9) are studied. Particularly the effects on the *cordons sanitaires* threshold (t_1^-) and eradication threshold (t_1^+) are studied.

Figure 4.8 shows that given a Patch 2 having a local basic reproductive number slightly bellow one ($\mathscr{R}_{02} = 0.9$), any increase on mobility from safer patch ($t_2 > 0$), have detrimental effects on the control of EVD outbreak. This is reflected on an increased traveling level needed from residents on the high-risk population, to avoid an EVD epidemic. In other words, as t_2 increases, t_1 does it so, implying that null mobility from Patch 2 minimizes t_1^+.

In addition, whenever individuals are exposed to a high risk of infection for long periods, mobility from the safe region might frustrate the EVD control efforts, regardless how exhaustive they are. Simulations in Figure 4.8 shows that when mobility from the safe region goes beyond $t_2 \approx 0.23$, there is no mobility from the high-risk region (t_1) capable to reduce the global $\mathscr{R}_0$ bellow one. Figure 4.9 shows that this threshold value depends on Patch 2 sanitary conditions.
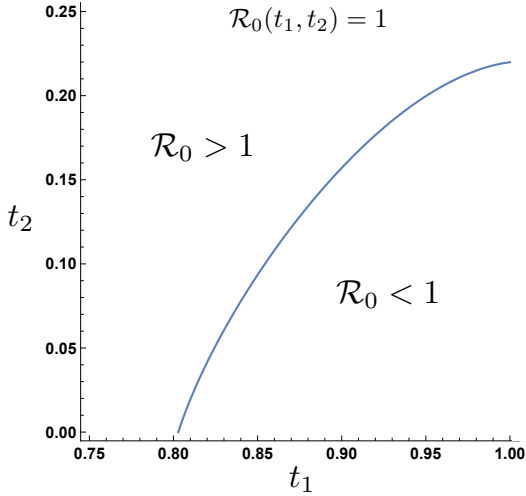
Figure 4.8: Level curve $\mathscr{R}_0(t_1, t_2) = 1$, for $\mathscr{R}_{02} = 0.9$.
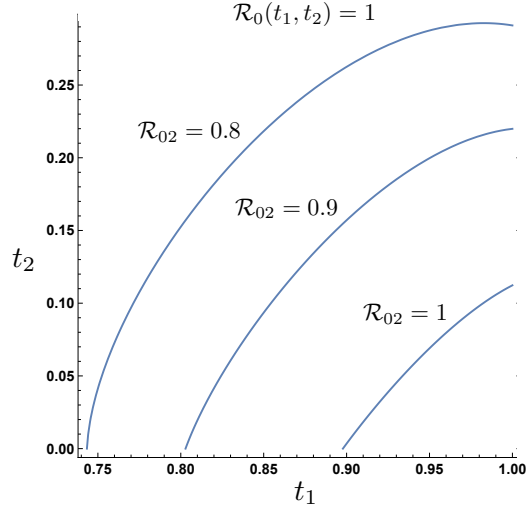
Figure 4.9: Level curves of $\mathscr{R}_0(t_1, t_2) = 1$ for $\mathscr{R}_{02} = 1, 0.9$ and 0.8.

Opposite to the case when the safe region have a local basic reproductive number slightly bellow one (Figures 4.8 and 4.9), extremely safe regions shows a different behavior in terms of the mobility needed to mathematically control an EVD outbreak. Simulations in Figure 4.10, suggest that null mobility from the safer patch to the high-risk region does not always minimize the mobility from the high-risk zone required to eradicate and EVD outbreak, (t_1^+).
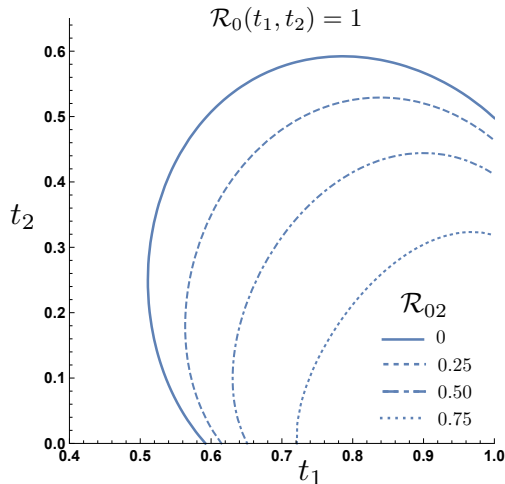
Figure 4.10: Level curves $\mathscr{R}_0(t_1, t_2) = 1$, for $\mathscr{R}_{02} = 0, 0.25, 0.5$ and 0.75.
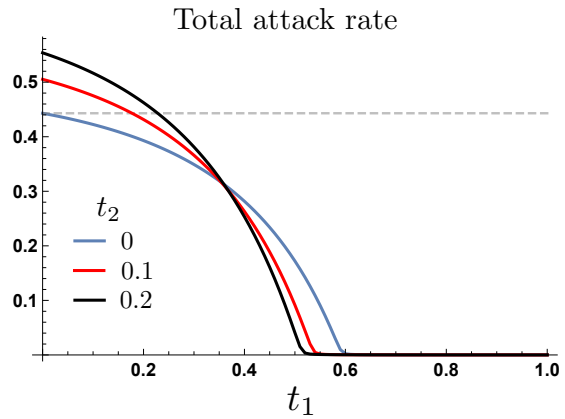
Figure 4.11: Attack rates under two ways mobility.

The total attack rate when almost no secondary infections are produced in the safe patch ($\mathscr{R}_{02} \approx 0$), is shown in Figure 4.11. The dynamics of the total attack rate as function of Patch 1 traveling level, for the Patch 2 mobility scenarios $t_2 = 0, 0.1$ and 0.2, under the extreme case $\mathscr{R}_{02} \approx 0$ are explored. For low t_1 values ($t_1 \approx 0$), the total attack rate increases as t_2 does it so. Nonetheless, for "high enough" t_1 values the total attack rate decreases faster for $t_2 = 0.2$, decreasing t_1^+, the mobility regime from the high-risk region required to control an ongoing EVD outbreak. As seen in Figure 4.10, the t_2 value that minimize t_1, is dependent on the $\mathscr{R}_{02}$.
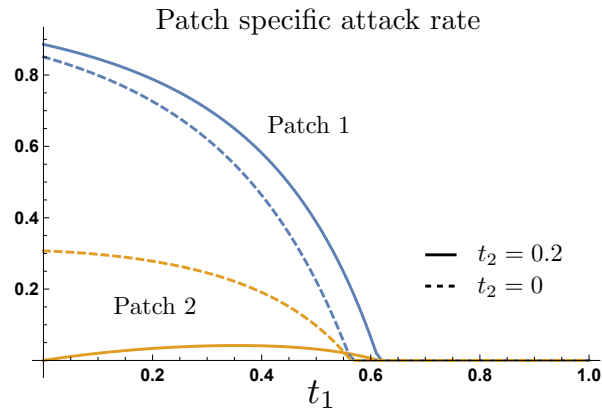
Figure 4.12: Visitant population breaks transmission chains in Patch 1.

Although previous result seems to be counter intuitive, Figure 4.12 contrast the dynamics of the patch-specific attack rate under safe region mobility levels of $t_2 = 0$ and $t_2 = 0.2$. The benefit obtained by allowing individuals from the safe region spend time in the high-risk region can be explained in terms of the trade-off between generating secondary infections among the high-risk patch individuals and generating secondary infections among the low-risk patch inhabitants. Since the epidemic in this polarized scenario is mainly driven by infections among Patch 1 individuals, reducing the high-risk region attack rate, also reduces the low-risk attack rate significantly. Thus, resulting on a beneficial trade off at high mobility levels.

In summary, null mobility from the safe-risk to high-risk area is not always the best strategy when the goal is to minimize the number of infected individuals. Particularly, for "small" differences in the patch-specific risks of infection, one way traveling seems to be the best strategy. In counterpart, when the system is composed by two regions having very notable disparities in infection risks, a two ways mobility strategy aimed to minimize the final number of infected individuals might be appealing.

4.5.3 The Effects of Patch Density Disparities

In this section, the impact of population density inequalities on the dynamics of EVD over a two-patch setting involving distinct infection risks is explored. Particularly, this section focus on the effects of populations' density ratio on both the mobility needed to reduce the final epidemic size bellow the *cordons sanitaires* threshold, and the mobility levels capable to eradicate an ongoing EVD outbreak.

Similar to Figure 4.6, where $N_1 = N_2$, Figure 4.13 shows the level curves dividing the $(\mathscr{R}_{02}, t_1)$ plane on regions where mobility and risk conditions either, increase or reduce the total final epidemic size, contrasted to the *cordons sanitaires* scenario. The curves in Figure 4.13 correspond to populations' ratios $\frac{N_1}{N_2} = k = 10, 1, \frac{1}{10}$. It is clearly seen that the region $\mathscr{R}_{02} < 0.35$, corresponding to the risk-mobility conditions where the *cordons sanitaires* strategy is not effective, is independent on the populations' densities. In counterpart, the regions where the *cordons sanitaires* control measure works or conditionally works are strongly affected by the populations' densities. Figure 4.13 simulations show that as the safe population's density increases, the mobility levels required to drop the total attack rate bellow the *cordons sanitaires* level, also increases. Thus, increasing the effectiveness of the *cordons sanitaires* as a control measure.

According to the model (4.7), for a safe population neighboring a smaller high-risk of infection zone, implementation of the *cordons sanitaires* might represent the best con-

tainment strategy, provided it cannot offer a "highly enough" safety level. For instance, in Figure 4.13, for population's densities $N_1 = 10N_2$, mobility from high risk region can reduces the total final size provided Patch 2 has a local basic reproductive number bellow the corresponding of the high-risk patch, $\mathscr{R}_{02} < \mathscr{R}_{01}$.
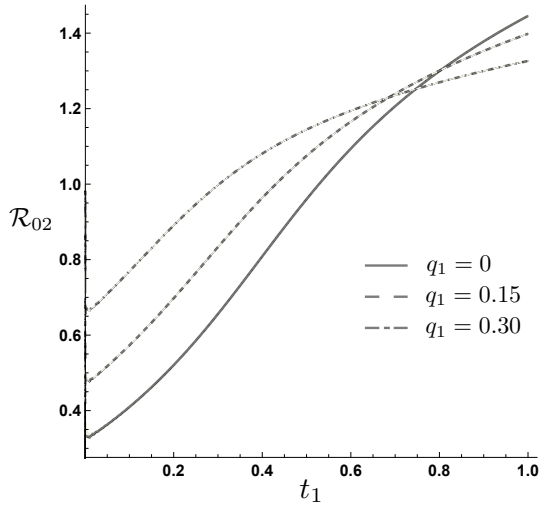
Figure 4.13: *Cordons Sanitaires* level curves for populations ratios $\frac{N_1}{N_2} = \frac{1}{10}, 1, 10$.
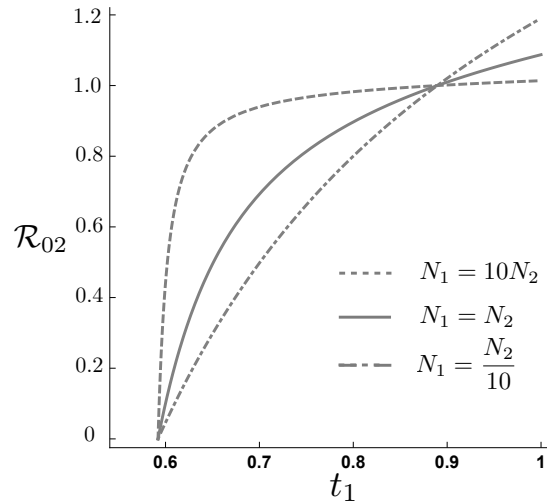
Figure 4.14: Level curve $\mathscr{R}_0(t_1, \mathscr{R}_{02}) = 1$, for populations ratios $\frac{N_1}{N_2} = \frac{1}{10}, 1, 10$.

Figure 4.14 exhibits how differences on population sizes affects the control of EVD in a two patch system with different risk environments. Simulations suggest that the more aggregated is the total population in the high-risk patch ($N_1 = 10N_2$), the traveling needed from this region to lead the global basic reproductive number bellow the unit, becomes less sensitive to the Patch 2 infection risk. Under this scenario, the EVD outbreak can be controlled via mobility from the high-risk patch, provided the classical threshold $\mathscr{R}_{02} < 1$ is hold and mobility above 60% is attained. On the other hand, as the total population aggregates in the safer patch ($N_1 = \frac{1}{10}N_2$), the traveling required to control an EVD epidemic becomes more sensitive to changes in Patch 2 infectiousness level, $\mathscr{R}_{02}$.

Since extreme cases are always illustrative, Figure 4.15 exhibits the dynamics of t_1^- threshold for two populations having extremely different densities. Not surprisingly, the

denser the safe population compared to the high-risk region, the mobility required to take the final epidemic size bellow the no mobility case is highly sensitive to the Patch 2 infection risk ($\mathscr{R}_{02}$). Moreover, as population aggregates in the safe region ($N_1 = \frac{1}{1,000}N_2$), the Patch 2 sanitary conditions ($\mathscr{R}_{02}$) making the *cordons sanitaires* an effective control strategy, converge to the sharp threshold $\mathscr{R}_{02} = 1$. On the other hand, when the total population is mainly aggregated in the high-risk patch ($N_1 = 1,000N_2$), the *cordons sanitaires* strategy becomes less effective, and almost all mobility level reduce the final epidemic size. Interestingly, when the population aggregates in the high-risk region ($N_1 = 1,000N_2$), the sanitary level required in Patch 2 converges to $\mathscr{R}_{02} \approx 3$.
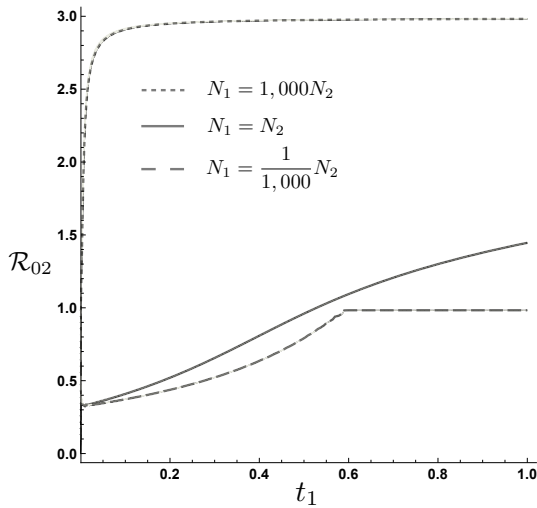
Figure 4.15: Extreme aggregation scenarios, shows convergence of mobility thresholds.
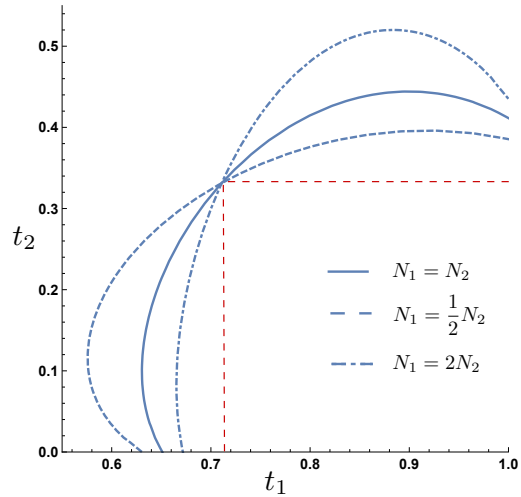
Figure 4.16: Level curves $\mathscr{R}_0(t_1,t_2) = 1$, for populations ratios $\frac{N_1}{N_2} = \frac{1}{2}, 1, 2$ and $\mathscr{R}_{02} = 0.5$.

Figure 4.16 shows the effects of populations' density disparities on the threshold condition $\mathscr{R}_0(t_1,t_2) = 1$. Simulations suggest that population aggregating in the safe patch makes a two ways mobility strategy more appealing in order to reduce the global basic reproductive number bellow one. Under the scenario $N_1 = \frac{1}{2}N_2$ and $\mathscr{R}_{02} = 0.5$, Patch 2 mobility of around 10%, reduces t_1^+ bellow 60%. On the other hand, Patch 2 null mobility requires a t_1^+ above 0.6 to attain a global $\mathscr{R}_0$ less than one. Population aggregation in the high-risk

patch ($N_1 = 2N_2$) allow more mobility from Patch 2, but it increases t_1^+, complicating the control of an EVD outbreak.

The red lines in Figure 4.16, denoting $t_1 \approx 0.7$ and $t_2 \approx 0.3$ shows the minimum Patch 1 and maximum Patch 2 traveling levels leading the global $\mathscr{R}_0$ bellow one (for $\mathscr{R}_{02} = 0.5$), regardless of the populations' density ratio. This is, there exist a pair of mobility thresholds independent of the populations' densities that mathematically drives $\mathscr{R}_0$ bellow one. These mobility thresholds are uniquely determined by the local basic reproductive numbers. However, as previously illustrated, when populations densities are also considered, a series of mobility strategies produced the desired effect on the global basic reproductive number..

4.6   Conclusion and Discussion

By using a two-patch model incorporating differences in risks of infection it was showed that mobility might work as an EVD control measure. In the studied polarized world, allowing residents from the high-risk region spend time in the safer area can ameliorate the overall impact of an epidemic. Results suggest that low mobility levels from the high-risk region tend to increases the total final epidemic size, while high mobility levels are capable to reduce it. Particularly, in absence of mobility from the low-risk region, allowing individuals from the high-risk zone spend more than 60% of their time sojourning in the safer patch can lead to EVD eradication.

Contrary to what is expected, simulations suggests that null mobility from the safer patch is not always harmful in terms of the final number of EVD cases. Whenever the low-risk patch has an exceptional capacity to respond against EVD infections, mobility from the low-risk region is capable to reduce the traveling level required from the highly affected population, in order to ameliorate the EVD burden. This can be explained as the effect of the visitant individuals breaking transmission chains within the high-risk region, importing

54

the disease into the safe patch and producing (on average) less secondary infections in this region. However, this strategy has the potential to boost the epidemic if the mobility from the highly affected patch is not high enough.

Finally, it was found that the time of residency needed outside the high-risk patch capable to produce a beneficial effect is highly dependent on the populations' density ratio. For the scenario where the population is mainly aggregated in a EVD low-risk of infection region, the *cordons sanitaires* control strategy will be effective whenever the epidemic cannot be locally contained in Patch 2 ($\mathscr{R}_{02} > 1$). On the other hand, for a population strongly aggregated in a high-risk region, allowing traveling to the safer patch will produce a benefit for almost all mobility levels. Additionally, the local risks of infection ($\mathscr{R}_{0i}$) implicitly define a set of traveling regimes thresholds after which an EVD epidemic is mathematically not sustainable, regardless of the populations' densities ratio.

It is worth to stress that in the presented work, the traveling time is assumed constant during the epidemic. Modeling the effects of social response to an epidemic goes beyond the scope of the presented work. Avoidance of contacts with EVD-infected individuals and EVD-infected corpses, as well as other control measures (quarantine, for instance), potentially reduce the exhibited thresholds mathematically leading to the control of an EVD epidemic.

Chapter 5

DYNAMICS OF THE CONTROL OF EVD ON HETEROGENEOUS RISK

ENVIRONMENTS IN THE PRESENCE OF MOBILITY

5.1   Introduction

Despite improvements in appropriately manage or possibly prevent an eventual new Ebola Virus Disease (EVD) outbreak, vulnerable African regions are still highly prone to future spillovers. Due to the absence of prophylactic and post-exposure EVD treatment on humans, EVD containment efforts lie on clinical management of patients, and prompt diagnose and isolation of infected individuals (Matua et al., 2015; A. Maxmen, 2017; Feldmann, 2010). The persistent EVD outbreaks on the African vulnerable regions demonstrate the necessity to implement long-term control efforts at individual, institutional and regional scales (Matua et al., 2015). The highly connected West African communities, mainly dependent on the local commerce, translate the EVD control into a regional rather than a local problem (Sorichetta et al., 2016; Blackwood and Childs, 2016). The work by Blackwood for example, addressed the role of localized control measures in a two patch setting by studying the impact of quarantine, hospitalization and burial practices in the presence of mobility. Authors found that regional connectivity substantially impacts control strategy effectiveness (Blackwood and Childs, 2016). The framework used differs from the Lagrangian approach used in the present work, since it does not track individuals' residency as they move across patches, nor considers the effective population sojourning in each region at a given time, i.e. residents plus visitant individuals.

The presented work aims to understand the impact of localized control measures on the dynamics of EVD, on a two-patch landscape where regions exhibit highly distinct risk

of EVD infection. The joint effects of short term mobility and, early detection and quar-antine of pre-symptomatic individuals is studied. The system is coupled by monitoring individuals' proportion of time spent sojourning in each region, while keeping their iden-tity according to its place of residency. Section 5.2, introduces the single patch EVD model explicitly modeling quarantine, along with the corresponding basic reproductive number and parameters used in simulations. In Section 5.3, a two-patch model coupled via resi-dence times is derived by extending the single patch model in section 5.2. Section 5.4 is devoted to the analysis of the proposed two-patch model. Specifically, the derivation of the global basic reproductive number and final epidemic size relation is done. In Section 5.5, main results obtained by numerically explore the proposed two-patch model are presented.

5.2   Model Derivation

The population studied is assumed to be constant over time and structured according to individuals' epidemiological states. It is assumed that a fraction of the infected popula-tion can be tested via RT-PCR assays to determine up to three days before symptoms onset whether their are infected or not. The total population is composed by susceptible individ-uals (S), latent undetectable individuals (E_1), latent detectable individuals (E_2), infected in-dividuals (I), quarantined infected individuals (Q), EVD-infected corpses (D), and removed individuals composed by recovered individuals and properly buried corpses (R). The total population (including buried and dead individuals) is then $N = S + E_1 + E_2 + I + Q + D + R$. The contagion process decreases the susceptible population by infections due to susceptible individuals (S) having contacts with infected individuals (I), quarantined infected individu-als (Q) or EVD-infected corpses (D), at rate $\beta \left(\frac{I + \varepsilon D + lQ}{N} \right)$. Latent individuals are assumed to be detectable via RT-PCR test on average $\frac{1}{\kappa_1}$ days after being infected, and become infec-tious on average after a period of $\frac{1}{\kappa_1} + \frac{1}{\kappa_2}$ days. During the second latency stage a fraction q of pre-symptomatic individuals are diagnosed and taken to isolation, while the rest are

neither detected nor isolated. Non-isolated infected individuals either die with probability f_d or recover after a mean period of $\frac{1}{\gamma}$ days.

EVD-infected corpses (D) before removed, on average after $\frac{1}{\nu}$ days, exhibit the highest viral load, then in the present work, these are assumed to be more infectious than infected individuals, ($\varepsilon > 1$). Finally, quarantined infected individuals are assumed to have a reduced infectious rate ($l \leq 1$), and recover after a mean period of $\frac{1}{\gamma}$. EVD-infected corpses produced while on quarantine are assumed to be properly removed from the system immediately, and do not contribute to the infectious process.

During the West African Ebola outbreak asymptomatic individuals associated to low viral loads were detected (Leroy et al., 2000). This possibility had antecedents during the Sudan (1976) and Zaire (1979) EVD outbreaks, where patients with symptoms ranging from mild, severe and rapidly fatal were noticed. (of a WHO/International Study Team et al., 1978). In this work, asymptomatic individuals having low viral loads are assumed incapable to produce secondary infections.

Population transitions through the EVD disease stages are showed in Figure 5.1
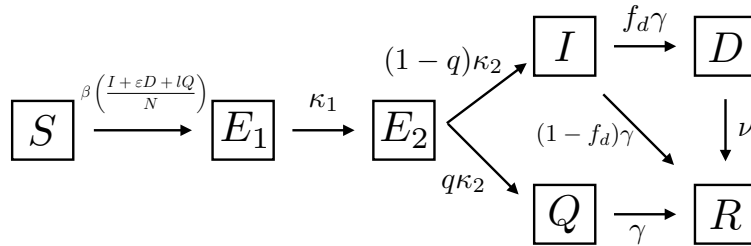
Figure 5.1: Ebola compartmental model with quarantine intervention.

and mathematically described by the system of ordinary differential equations (5.1)

$$
\begin{cases}
N = S + E_1 + E_2 + I + Q + D + R \\
\dot{S} = -\beta S \left(\frac{I + \varepsilon D + lQ}{N} \right) \\
\dot{E_1} = \beta S \left(\frac{I + \varepsilon D + lQ}{N} \right) - \kappa_1 E_1 \\
\dot{E_2} = \kappa_1 E_1 - \kappa_2 E_2 \\
\dot{I} = (1 - q)\kappa_2 E_2 - \gamma I \\
\dot{Q} = q\kappa_2 E_2 - \gamma Q \\
\dot{D} = f_{\mathrm{d}}\gamma I - \nu D \\
\dot{R} = (1 - f_{\mathrm{d}})\gamma I + \nu D + \gamma Q
\end{cases}
\tag{5.1}
$$

The basic reproductive number $\mathscr{R}_0$ represents the number of secondary infections by an infected individual in an essentially susceptible population in absence of control measures. In counterpart, the control reproductive number $\mathscr{R}_c$, quantify the number of secondary infections caused by a single infected individual in a susceptible population under the effects of control measures. Then, the control reproductive number determines the beginning of the recognition of the epidemic. For model (5.1), the control and basic reproductive number are given by

$$
\mathscr{R}_c = q\mathscr{R}_Q + (1 - q)\mathscr{R}_0
\tag{5.2}
$$

where the quarantine reproductive number $\mathscr{R}_Q = \dfrac{l\beta}{\gamma}$, captures the secondary infections produced by a typical individual in quarantine, and the basic reproductive number $\mathscr{R}_0 = \beta \left(\dfrac{1}{\gamma} + \dfrac{f_d \varepsilon}{\nu} \right)$ captures the secondary infections produced by infected individuals and non-removed infected EVD-infected corpses in absence of control intervention. Explicitly, the control reproductive number accounts for the secondary infections produced by the proportion of diagnosed pre-symptomatic individuals (q) during its infectious period $\left(\frac{1}{\gamma} \right)$ at a reduced infectiousness ($l\beta$), secondary infections produced by non isolated infectious individuals ($1 - q$) during their infectious period $\left(\frac{1}{\gamma} \right)$ at the baseline infectiousness (β), and

secondary infections produced by non-quarantined EVD-infected corpses ($(1-q)f_d$) with increased infectiousness ($\varepsilon\beta$) during its average disposal time $\left(\frac{1}{v}\right)$.

$$\mathscr{R}_c = q\left(\frac{l\beta}{\gamma}\right) + (1-q)\beta\left(\frac{1}{\gamma} + \frac{f_d\varepsilon}{v}\right). \tag{5.3}$$

Model parameters were directly extracted from literature. The mean incubation period $\left(\frac{1}{\kappa}\right)$ is assumed to be 7 days (Legrand et al., 2007; Ndambi et al., 1999). It has been estimated from previous EVD outbreaks a mean period from symptoms onset to the end of infectiousness $\left(\frac{1}{\kappa}\right)$ of 7 days (Chowell and Nishiura, 2014; Chowell et al., 2015). The average time it takes health care workers to properly bury EVD-infected corpses, i.e. EVD-infected corpses infectious period, has been estimated of about 2 days (Legrand et al., 2007). EVD fatality rate has a great range of fatality, going from 50% to 90%. In this work EVD fatality rate is assumed to be of 70% (Chowell and Nishiura, 2014). EVD-infected corpses are assumed to have the maximum viral load, thus being more infectious than infected individuals, and captured by $\varepsilon > 1$. The parameter β has been calibrated to approximate model's (5.1) basic reproduction number to $\mathscr{R}_0 \approx 2.45$ (Althaus, 2014; Chowell et al., 2004). Quarantine capacity (q) and quarantined infected individuals relative infectiousness (l) varies between $[0,1]$ in order to explore their effects on the EVD dynamics. Table 5.1, summarize the parameters used to calibrate simulations done in this work.

Table 5.1: Parameters of the single patch EVD model.

Parameter	Description	Base model values	
β	Per susceptible infection rate	0.287	(Althaus, 2014)
γ	Rate at which an infected recovers or dies	1/7	(Team, 2014)
κ_1	Per-capita progression rate to latent detectable stage	1/4	(Legrand et al., 2007)
κ_2	Per-capita progression rate from latent detectable to infectious stage	1/3	(Towner et al., 2004)
v	Per-capita body disposal rate	1/2	(Legrand et al., 2007)
f_d	Proportion of infected who die due to infection	0.7	(Team, 2014)
ε	Scale: Ebola infectiousness of dead bodies	>1	(Li et al., 2016)
q	Proportion of latent individuals diagnosed before symptoms onset	[0,1]	
l	Isolated individuals relative transmissibility	[0,1]	

5.3 Ebola Dynamics on Heterogeneous Risk Environments

Assessing the effectiveness of localized control measures imposed on a population during an epidemic is not a trivial task. While mathematical models simplify the real world situation, many factors modulate the observed output. Populations' mobility, beliefs and education are some of the important factors in the context of designing appropriate control measures to fight Ebola. The reduction on EVD transmission at the time interventions were introduced in Sierra Leone, between June 2014 and February 2015 has been studied (Kucharski et al., 2015). Despite the difficulty of assessing the direct impact of a particular control measure, authors focused on estimate the cases prevented by increasing treatment beds available in different districts. Blackwood for example, by studying the impact of quarantine, hospitalization and burial practices in presence of mobility, addressed the impact of localized control measures in a two-patch setting on the control of an epidemic (Blackwood and Childs, 2016). Although the framework used does not incorporates the role of the effective population sojourning in a given patch at a particular time, authors found that regional connectivity substantially affects control strategy effectiveness.

In this work, by using the Lagrangian approach through residency, specifically the mobility matrix $\mathbb{P}$, individuals' preserving their place of residency are tracked at all time across patches (Bichara et al., 2015). Thus, the average effective density of individuals sojourning in Patch i, which is composed by the expected amount of residents individuals sojourning in Patch i at time t ($p_{ii}N_i$), and the expected visitant individuals ($p_{ji}N_j$). On a two-patch landscape where infections are produced uniquely by infected individuals, the number of

new infections within Patch j residents is expressed by

$$\varphi(j) = \underbrace{\beta_i}_{\text{Patch } i \text{ infection risk}} \underbrace{p_{ji}S_j}_{\text{Expected Patch } j \text{ susceptible pop. in Patch } i} \underbrace{\frac{p_{ii}I_i + p_{ji}I_j}{p_{ii}N_i + p_{ji}N_j}}_{\text{Proportion of infected pop. in Patch } j}$$

$$+ \underbrace{\beta_j}_{\text{Patch } j \text{ infection risk}} \underbrace{p_{jj}S_j}_{\text{Expected Patch } j \text{ susceptible pop. in Patch } j} \underbrace{\frac{t_i I_i + p_{jj}I_j}{p_{ij}N_i + p_{ji}N_j}}_{\text{Proportion of infected pop. in Patch } j}$$

$$(5.4)$$

this is, Patch j residents can get infected while sojourning in Patch i (with corresponding risk of infection β_i) and at their patch of residency (with associated risk of infection β_j). Note that the times of residency of Patch i residents traveling in a n-patch landscape should hold $\sum_{j=1}^{n} p_{ij} = 1$.

In the context of Ebola, infections caused by EVD-infected corpses or quarantined individuals are assumed to only occur within their patch of residency. Moreover, quarantined individuals, similar to EVD-infected corpses, are assumed not to be transported across patches. Thus, the Patch j population capable to travel is approximated by monitoring the time of residency of non quarantined individuals in Patch i, $(1 - q_j)p_{ji}N_j$. New EVD cases among Patch j residents are assumed to occur by infections produced within Patch j, by having contacts with residents and visitant infected individuals, and resident EVD-infected corpses and quarantine individuals, at rate

$$\beta_j p_{jj} S_j \left(\frac{p_{ij}I_i + p_{jj}I_j}{(1 - q_i)p_{ij}N_i + p_{jj}N_j} + \frac{\varepsilon_j D_j + l_j Q_j}{N_j} \right) \tag{5.5}$$

or by Patch j residents having contacts with residents and visitor infected individuals in Patch i, at rate

$$\beta_i p_{ji} S_j \left(\frac{p_{ii}I_i + p_{ji}I_j}{p_{ii}N_i + (1 - q_j)p_{ji}N_j} \right). \tag{5.6}$$

Hence (5.4), becomes

$$\beta_j p_{jj} S_j \left(\frac{p_{ij}I_i + p_{jj}I_j}{(1-q_i)p_{ij}N_i + p_{jj}N_j} + \frac{\varepsilon_j D_j + l_j Q_j}{N_j} \right) + \beta_i p_{ji} S_j \left(\frac{p_{ii}I_i + p_{ji}I_j}{p_{ii}N_i + (1-q_j)p_{ji}N_j} \right)$$
(5.7)

In this work, the notation used to monitor individual's times of residency on a two-patch landscape is simplified by tracking individuals' "traveling time", the time a typical Patch i individual spend visiting Patch j, t_i. Patch i residents' average proportion of traveling time is denoted by t_i, while $1 - t_i$ denotes the average proportion of time spent on their own patch. Therefore (5.7) takes the form

$$\beta_j(1-t_j)S_j \left(\frac{t_i I_i + (1-t_j)I_j}{(1-q_i)t_i N_i + (1-t_j)N_j} + \frac{\varepsilon_j D_j + l_j Q_j}{N_j} \right) + \beta_i t_j S_j \left(\frac{(1-t_i)I_i + t_j I_j}{(1-t_i)N_i + (1-q_j)t_j N_j} \right)$$
(5.8)

By following the construction of model (5.1) and the infection force (5.8), the two-patch model incorporating quarantine and residency times can be written as

$$
\begin{cases}
N_i = S_i + E_{i1} + E_{i2} + I_i + Q_i + D_i + R_i \\[4pt]
\dot{S}_i = -(1-t_i)\beta_i S_i \left(\frac{(1-t_i)I_i + t_j I_j}{(1-t_i)N_i + (1-q_j)t_j N_j} + \frac{\varepsilon D_i + l_i Q_i}{N_i} \right) - t_i \beta_j S_i \left(\frac{t_i I_i + (1-t_j)I_j}{(1-q_i)t_i N_i + (1-t_j)N_j} \right) \\[4pt]
\dot{E}_{i1} = (1-t_i)\beta_i S_i \left(\frac{(1-t_i)I_i + t_j I_j}{(1-t_i)N_i + (1-q_j)t_j N_j} + \frac{\varepsilon D_i + l_i Q_i}{N_i} \right) + t_i \beta_j S_i \left(\frac{t_i I_i + (1-t_j)I_j}{(1-q_i)t_i N_i + (1-t_j)N_j} \right) - \kappa_1 E_{i1} \\[4pt]
\dot{E}_{i2} = \kappa_1 E_{i1} - \kappa_2 E_{i2} \\[4pt]
\dot{I}_i = (1-q_i)\kappa_2 E_{i2} - \gamma I_i \\[4pt]
\dot{Q}_i = q_i \kappa_2 E_{i2} - \gamma Q_i \\[4pt]
\dot{D}_i = f_{\mathrm{d}}\gamma I_i - v_i D_i \\[4pt]
\dot{R}_i = (1-f_{\mathrm{d}})\gamma I_i + v D_i + \gamma Q_i
\end{cases}
$$
(5.9)

5.4   Model Analysis

In this section the control and basic reproductive numbers, as well as the patch-specific and total final epidemic size relations are analytically derived.

5.4.1 Computation of the Basic and Control Reproductive Numbers on Heterogeneous Risk Environments

System (5.9) control and basic reproduction numbers are computed by following the next generation approach (Diekmann et al., 1990; van den Driessche and Watmough, 2002). Consider the infectious compartments E_{11}, E_{12}, I_1, Q_1, D_1, E_{21}, E_{22}, I_2, Q_2 and D_2, which evaluated at the disease free equilibrium leads to $S_1(0) = N_1$ and $S_2(0) = N_2$, then

$$
\mathscr{F} = \begin{pmatrix}
(1-t_1)\beta_1 S_1 \left(\frac{(1-t_1)I_1+t_2 I_2}{(1-t_1)N_1+(1-q_2)t_2 N_2} + \frac{\varepsilon D_1+l_1 Q_1}{N_1} \right) + t_1 \beta_2 S_1 \left(\frac{t_1 I_1+(1-t_2)I_2}{(1-q_1)t_1 N_1+(1-t_2)N_2} \right) \\
0 \\
0 \\
0 \\
0 \\
(1-t_2)\beta_2 S_2 \left(\frac{t_1 I_1+(1-t_2)I_2}{(1-q_1)t_1 N_1+(1-t_2)N_2} + \frac{\varepsilon D_2+l_2 Q_2}{N_2} \right) + t_2 \beta_1 S_2 \left(\frac{(1-t_1)I_1+t_2 I_2}{(1-t_1)N_1+(1-q_2)t_2 N_2} \right) \\
0 \\
0 \\
0 \\
0
\end{pmatrix}
$$

and

$$\mathcal{V} = \begin{pmatrix} \kappa_1 E_{11} \\ -\kappa_1 E_{11} + \kappa_2 E_{12} \\ -(1-q_1)\kappa_2 E_{12} + \gamma I_1 \\ -q_1 \kappa_2 E_{12} + \gamma Q_1 \\ -f_d \gamma I_1 + v_1 D_1 \\ \kappa_1 E_{21} \\ -\kappa_1 E_{21} + \kappa_2 E_{22} \\ -(1-q_2)\kappa_2 E_{22} + \gamma I_2 \\ -q_2 \kappa_2 E_{22} + \gamma Q_2 \\ -f_d \gamma I_2 + v D_2 \end{pmatrix}.$$

Thus the second generation matrix is composed by

$$F = \left(\begin{array}{c|c} J_1 & K_1 \\ \hline K_2 & J_2 \end{array} \right)$$

where

$$J_i = \begin{pmatrix} 0 & 0 & M_i & A_i & B_i \\ 0 & 0 & 0 & 0 & 0 \\ 0 & 0 & 0 & 0 & 0 \\ 0 & 0 & 0 & 0 & 0 \\ 0 & 0 & 0 & 0 & 0 \end{pmatrix}, \qquad K_i = \begin{pmatrix} 0 & 0 & C_i & F_i & G_i \\ 0 & 0 & 0 & 0 & 0 \\ 0 & 0 & 0 & 0 & 0 \\ 0 & 0 & 0 & 0 & 0 \\ 0 & 0 & 0 & 0 & 0 \end{pmatrix},$$

and

$$M_i = \frac{N_i(1-t_i)^2 \beta_i}{(1-t_i)N_i + t_j N_j} + \frac{t_i^2 N_i \beta_j}{(1-t_i)N_i + t_j N_j}, \quad A_i = \frac{(1-t_i)N_i l_i \beta_i}{(1-t_i)N_i + t_j N_j}, \quad B_i = \frac{(1-t_i)N_i \varepsilon \beta_i}{(1-t_i)N_i + t_j N_j},$$

$$C_i = \frac{(1-t_i)N_i t_j \beta_i}{(1-t_i)N_i + t_j N_j} + \frac{t_i(1-t_j)N_i \beta_j}{t_i N_i + (1-t_j)N_j}, \quad F_i = \frac{t_i N_i l_j \beta_j}{t_i N_i + (1-t_j)N_j}, \quad G_i = \frac{t_i N_i \varepsilon_j \beta_j}{t_i N_i + (1-t_j)N_j},$$

and

$$V = \left(\begin{array}{c|c} H_1 & 0_{5\times5} \\ \hline 0_{5\times5} & H_2 \end{array} \right)$$

65

where

$$H_i = \begin{pmatrix} \kappa_1 & 0 & 0 & 0 & 0 \\ -\kappa_1 & \kappa_2 & 0 & 0 & 0 \\ 0 & -(1-q_i)\kappa_2 & \gamma & 0 & 0 \\ 0 & -q_i\kappa_i & 0 & \gamma & 0 \\ 0 & 0 & -f_d\gamma & 0 & v \end{pmatrix}.$$

The basic reproduction number is finally, the spectral radius of the next generation matrix $-FV^{-1}$ given by

$$-FV^{-1} = \begin{pmatrix} \phi_1 & \phi_1 & \frac{B_1 f_d}{v} + \frac{M_1}{\gamma} & \frac{A_1}{\gamma} & \frac{B_1}{v} & \varphi_1 & \varphi_1 & \frac{C_1}{\gamma} + \frac{f_d G_1}{v} & \frac{F_1}{\gamma} & \frac{G_1}{v} \\ 0 & 0 & 0 & 0 & 0 & 0 & 0 & 0 & 0 & 0 \\ 0 & 0 & 0 & 0 & 0 & 0 & 0 & 0 & 0 & 0 \\ 0 & 0 & 0 & 0 & 0 & 0 & 0 & 0 & 0 & 0 \\ 0 & 0 & 0 & 0 & 0 & 0 & 0 & 0 & 0 & 0 \\ \varphi_2 & \varphi_2 & \frac{C_2}{\gamma} + \frac{f_d G_2}{v} & \frac{F_2}{\gamma} & \frac{G_2}{v} & \phi_2 & \phi_2 & \frac{B_2 f_d}{v} + \frac{M_2}{\gamma} & \frac{A_2}{\gamma} & \frac{B_2}{v} \\ 0 & 0 & 0 & 0 & 0 & 0 & 0 & 0 & 0 & 0 \\ 0 & 0 & 0 & 0 & 0 & 0 & 0 & 0 & 0 & 0 \\ 0 & 0 & 0 & 0 & 0 & 0 & 0 & 0 & 0 & 0 \\ 0 & 0 & 0 & 0 & 0 & 0 & 0 & 0 & 0 & 0 \end{pmatrix}$$

where

$$\phi_i = \frac{(1-q_i)M_i}{\gamma} + \frac{q_i A_i}{\gamma\kappa_2} + \frac{B_i f_d(1-q_i)}{v}, \quad \text{and} \quad \varphi_i = \frac{(1-q_j)C_i}{\gamma} + \frac{q_j F_i}{\gamma\kappa_2} + \frac{G_i f_d(1-q_j)}{v}.$$

Due to the expression length, the final output is avoided. However, numerical explorations of the control reproductive number are done in further sections.

5.4.2 EVD Final Epidemic Size on Heterogeneous Risk Environments

In this section, the overall and patch specific final epidemic size relations as functions of the patch residency times and local risks of infection are derived. To simplify notation,

the expressions $\hat{f}(t) = \int_0^\infty f(s)ds$ and $f^\infty = \lim_{t\to\infty} f(t)$, are used. Assume $S_i(0) = N_i$,

$E_{1i}(0) = E_{2i}(0) = I_i(0) = Q_i(0) = D_i(0) = 0$, then adding the first two equations of model

(5.1) leads to $\dot{S}_i + \dot{E}_{1i} = -\kappa_1 \hat{E}_{1i}$ and $E_{1i}^\infty = 0$. Following the same reasoning it is possible

to show that $E_{2i}^\infty = I_i^\infty = Q_i^\infty = D_i^\infty = 0$, $\hat{E}_{1i} = \frac{N_i - S_i^\infty}{\kappa_1}$, $\hat{E}_{2i} = \frac{N_i - S_i^\infty}{\kappa_2}$, $\hat{I}_i = (N_i - S_i^\infty)\frac{(1-q_i)}{\gamma}$,

$\hat{Q}_i = (N_i - S_i^\infty)\frac{q_i}{\gamma}$ and $\hat{D}_i = (N_i - S_i^\infty)\frac{(1-q_i)f_d}{v_i}$. Therefore, for each patch, the following

relations are obtained

$$\log\left(\frac{N_1}{S_1^\infty}\right) = (N_1 - S_1^\infty)\left((1-t_1)\beta_1\left(\frac{(1-t_1)\frac{1-q_1}{\gamma}}{(1-t_1)N_1 + (1-q_2)t_2N_2} + \frac{\varepsilon\frac{(1-q_1)f_d}{v_1} + l_1\frac{q_1}{\gamma}}{N_1}\right)\right.$$

$$+ t_1\beta_2\frac{(1-q_1)\frac{t_1}{\gamma}}{(1-q_1)t_1N_1 + (1-t_2)N_2}\right)$$

$$+ (N_2 - S_2^\infty)\left((1-t_1)\beta_1\frac{t_2\frac{1-q_2}{\gamma}}{(1-t_1)N_1 + (1-q_2)t_2N_2}\right.$$

$$+ t_1\beta_2\frac{(1-t_2)\left(\frac{1-q_2}{\gamma}\right)}{(1-q_1)t_1N_1 + (1-t_2)N_2}\right)$$

$$\log\left(\frac{N_2}{S_2^\infty}\right) = (N_1 - S_1^\infty)\left((1-t_2)\beta_2\frac{t_1\frac{1-q_1}{\gamma}}{(1-q_1)t_1N_1 + (1-t_2)N_2}\right.$$

$$+ t_2\beta_1\frac{(1-t_1)\left(\frac{1-q_1}{\gamma}\right)}{(1-t_1)N_1 + (1-q_2)t_2N_2}\right)$$

$$+ (N_2 - S_2^\infty)\left((1-t_2)\beta_2\left(\frac{(1-t_2)\frac{1-q_2}{\gamma}}{(1-q_1)t_1N_1 + (1-t_2)N_2} + \frac{\varepsilon\frac{(1-q_2)f_d}{v_2} + l_2\frac{q_2}{\gamma}}{N_2}\right)\right.$$

$$+ t_2\beta_1\frac{t_2\frac{1-q_2}{\gamma}}{(1-t_1)N_1 + (1-q_2)t_2N_2}\right)$$

which can be expressed in vector form as

$$
\begin{bmatrix} \log\left(\dfrac{N_1}{S_1^\infty}\right) \\[2mm] \log\left(\dfrac{N_2}{S_2^\infty}\right) \end{bmatrix} = \begin{bmatrix} B_{11} & B_{12} \\[1mm] B_{21} & B_{22} \end{bmatrix} \begin{bmatrix} 1-\dfrac{S_1^\infty}{N_1} \\[2mm] 1-\dfrac{S_2^\infty}{N_2} \end{bmatrix}
$$

where

$$
B_{11} = \left((1-t_1)\beta_1 \left(\frac{(1-t_1)\frac{1-q_1}{\gamma}}{(1-t_1)N_1+(1-q_2)t_2N_2} + \frac{\varepsilon\frac{(1-q_1)f_d}{v_1}+l_1\frac{q_1}{\gamma}}{N_1} \right) \right.
$$

$$
\left. + \ t_1\beta_2 \frac{(1-q_1)\frac{t_1}{\gamma}}{(1-q_1)t_1N_1+(1-t_2)N_2} \right) N_1,
$$

$$
B_{12} = \left((1-t_1)\beta_1 \frac{t_2\frac{1-q_2}{\gamma}}{(1-t_1)N_1+(1-q_2)t_2N_2} + t_1\beta_2 \frac{(1-t_2)\left(\frac{1-q_2}{\gamma}\right)}{(1-q_1)t_1N_1+(1-t_2)N_2} \right) N_2,
$$

$$
B_{21} = \left((1-t_2)\beta_2 \frac{t_1\frac{1-q_1}{\gamma}}{(1-q_1)t_1N_1+(1-t_2)N_2} + t_2\beta_1 \frac{(1-t_1)\left(\frac{1-q_1}{\gamma}\right)}{(1-t_1)N_1+(1-q_2)t_2N_2} \right) N_1
$$

$$
B_{22} = \left((1-t_2)\beta_2 \left(\frac{(1-t_2)\frac{1-q_2}{\gamma}}{(1-q_1)t_1N_1+(1-t_2)N_2} + \frac{\varepsilon\frac{(1-q_2)f_d}{v_2}+l_2\frac{q_2}{\gamma}}{N_2} \right) \right.
$$

$$
\left. + \ t_2\beta_1 \frac{t_2\frac{1-q_2}{\gamma}}{(1-t_1)N_1+(1-q_2)t_2N_2} \right) N_2.
$$

Note that, the final size relation on an n-patch system is given by a system of n equations, and is denoted by the patch-specific final proportion of infected individuals

$$
\begin{bmatrix} 1-\dfrac{S_1^\infty}{N_1} \\[2mm] 1-\dfrac{S_2^\infty}{N_2} \end{bmatrix},
$$

and the matrix B denoting the secondary infections produced by Patch i and Patch j secondary infections produced in each environment. For instance, for the presented two-patch

68

model, B_{12} captures Patch 1 residents' infections produced by having contacts with Patch 2 inhabitants. While spending $(1 - t_1)$ proportion of time at their patch of residency and by having contacts with infected visitant individuals $((1 - q_2)t_2)$

$$(1 - t_1)\beta_1 \frac{t_2 \frac{1 - q_2}{\gamma}}{(1 - t_1)N_1 + (1 - q_2)t_2N_2},$$

and, while visiting Patch 2 and being infected by contacts with Patch 2 non quarantined infected residents

$$t_1\beta_2 \frac{(1 - t_2)\left(\frac{1 - q_2}{\gamma}\right)}{(1 - q_1)t_1N_1 + (1 - t_2)N_2}.$$

Furthermore, it is important to stress that in the construction of the Lagrangian approach, the eigenvalues of the matrix B, on the final epidemic size relation, are the same of the second generation matrix. Particularly, $\mathcal{R}_C$ is also the spectral radius of B, (Bichara et al., 2015). Moreover, under the Lagrangian approach, the global control reproductive number is a function of the residence matrix ($\mathbb{P}$) and the local control reproductive numbers ($\mathcal{R}_{C1}$ and $\mathcal{R}_{C2}$), defined in absence of mobility ($t_1 = t_2 = 0$). Hence $\mathcal{R}_C = f(\mathbb{P}, \mathcal{R}_{C1}, \mathcal{R}_{C2})$.

5.5   Results

In this section the impact of individuals moving across patches (having distinct infectious risks) on the control interventions effectiveness is addressed. Particularly, this work focus on addressing questions such as, how mobility impacts the effectiveness of quarantine programs aimed to reduce EVD cases? does mobility increase or reduce the quarantine threshold required to properly manage EVD epidemic?

In order to address these questions a two-patch mathematical model assuming patch specific constant populations ($N_1 = N_2 = 10,000$), but having different risk of EVD infection, is studied. Patch 1 is assumed to represent a region having high-risk of infection and capable to sustain an EVD outbreak. Conditions in this patch are assumed to produce a high local basic reproductive number. Data from the West African EVD epidemic is used

to calibrate model (5.9) risk conditions to match $\mathscr{R}_{01} = 2.45$ (Towers et al., 2014; Chowell and Nishiura, 2014; Althaus, 2014). Patch 2 is assumed to exemplify a region incapable to sustain an EVD epidemic, having a low-risk of infection and a local basic reproductive number bellow the unit, $\mathscr{R}_{02} = 0.738$.

Some patch-specific conditions like social, economic and health characteristics lead to differences in risk of infection and are captured in a single parameter β_i. The contagion process is assumed to start by the introduction of an infected individual in Patch 1, and in the presence of mobility, the epidemic is capable to spread to Patch 2.

5.5.1 The Effect of Quarantine Pre-Symptomatic Individuals on the Spread of EVD on Distinct Risk Environments

In this section, numerical explorations aimed to assessing the effects of mobility on the global reproductive number and EVD total attack rate are performed. It is assumed that a fraction of the population (q), is opportunistically diagnosed and quarantined before symptoms onset.

Figures 5.2 and 5.3 show the effects of mobility from the high-risk region on the total and patch specific final epidemic size, in absence of control interventions, and when 20% of detected individuals are quarantine in Patch 1, respectively. Naturally, quarantine implementation in the high-risk region reduces the final epidemic size for all traveling scenarios. More interestingly, quarantine reduces the mobility needed to control an EVD outbreak by mobility from the high-risk region, i.e. making mobility management a more feasible control measure.
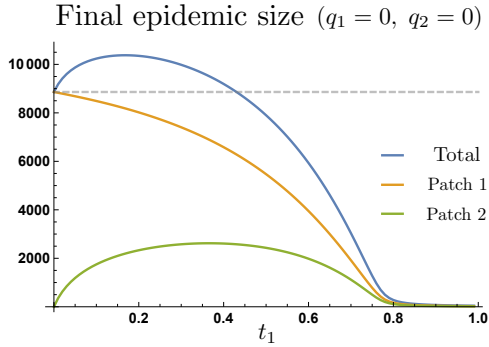
Figure 5.2: Total and patch specific final epidemic size under Patch 1 mobility, $q_1 = 0 = q_2$ and $\mathscr{R}_{01} = 0.9$.
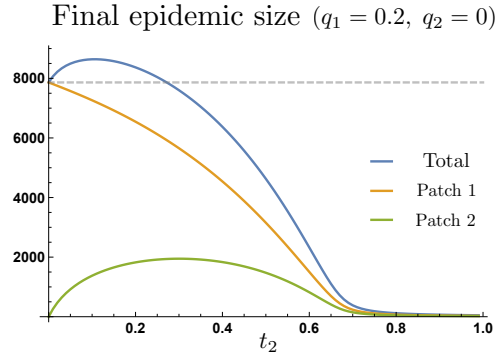
Figure 5.3: Total and patch specific final epidemic size under Patch 1 mobility, $q_1 = 0.2$, $q_2 = 0$ and $\mathscr{R}_{01} = 0.9$.

Isolation of infected individuals produces transmission chains breakage, decreasing the final epidemic size for all mobility levels. However, a more important effect of quarantine considerable proportions of the population is that this control measure impacts the effective population traveling across patches. This directly impact the traveling thresholds producing benefits in terms of the final epidemic size and controlling an EVD epidemic on the overall system.

Figure 5.4 shows the dynamics of the overall attack rate under scenarios where none, 20% and 35% of pre-symptomatic individuals are perfectly isolated ($l = 0$) and for $\mathscr{R}_{02} = 0.9$. Simulations suggest that detecting and quarantining a low proportion of the infected individuals in the high-risk region (for example, $q_1 = 0.2$) produces a significant reduction on the overall EVD attack rate. Although in the presence of quarantine, the *cordons sanitaires* scenario attack rate ($t_1 = 0$) decreases, quarantine low proportions of the infected individuals in Patch 1 ($q_1 \leq 0.35$) produces similar dynamics of the total attack rate as function of the Patch 1 mobility, i.e. the total attack rate increases for small traveling regimes. Nonetheless, quarantining a "big enough" proportion of infected individuals in the high-risk region, can vanish the detrimental effect of low mobility regimes, reshaping the total attack rate as a monotonic decreasing function as Patch 1 traveling increases.

Total attack rate

$\mathcal{R}_{02} = 0.9$

— $q_1 = 0$
---- $q_1 = 0.2$
–·– $q_1 = 0.35$

Total attack rate

$\mathcal{R}_{02} = 0.9$

— $q_2 = 0$
---- $q_2 = 0.25$
–·– $q_2 = 0.5$
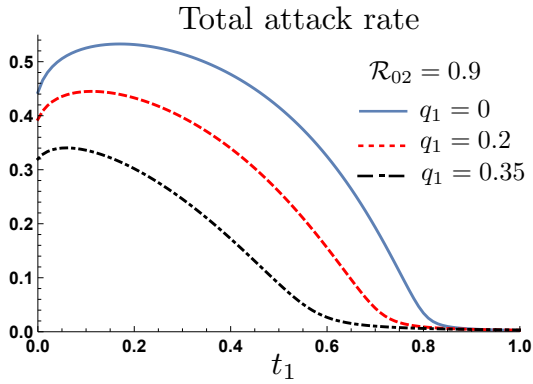
Figure 5.4: The total attack rate decreases dramatically as quarantine of pre-symptomatic individuals increases. All levels of Patch 1 residents mobility are beneficial if more than 35% pre-symptomatic individuals are under perfect isolation.
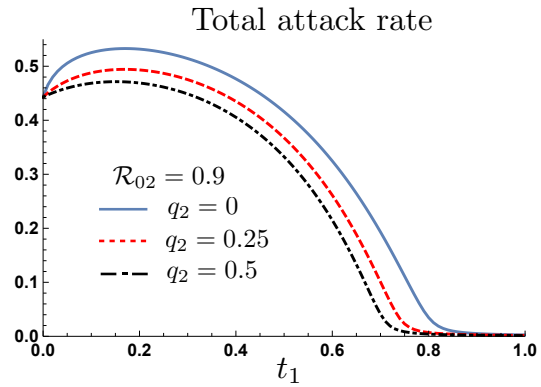
Figure 5.5: The total attack rate decreases by increasing quarantine in low-risk region. However, even Patch 2 big quarantine programs ($q_2 = 0.5$) slightly helps on controlling epidemic. $q_1 = 0.2$

On the other hand, Patch 2 quarantine interventions are not as effective as do it in the highly vulnerable region. Figure 5.5 shows that even implementing "big" quarantine programs in the safe region has not a significant impact in reducing the total attack rate, unless high mobility levels from the high-risk region are attained. Although the efficacy of the *cordons sanitaires* control strategy on reducing the total attack rate depends on both patches traveling regimes and quarantine programs, previous results show that quarantine programs and mobility from the high-risk population produce the major impacts on decreasing the total attack rate.

5.5.2   Quarantine vs Isolation on the containment of Ebola

In this section, the effects of isolation and quarantine on the dynamics of EVD on heterogeneous risk environments are numerically explored. Quarantine and isolation have been historically used as control measures aimed to contain the spread of communicable diseases. The mechanism upon these control strategies are based is simple, by reducing infected individuals' interactions with the rest of the population, the disease burden is ex-

72

pected to be reduced due to transmission chains breakage. Despite the wide historical use of these strategies on the control of diseases, their specific impacts and effectiveness are still controversial, being current sources of active research. The importance of understanding the dynamical consequences of implementing such control measures is exacerbated by situations where dealing with diseases for which there is no available vaccine or treatment. In such situations, quarantine and/or isolation become the only available control measures to arrest or mitigate, the epidemic. Addressing the precise definitions for isolation and quarantine as control measures, are historical challenges. Many of the modern research coincide in defining isolation as the segregation of individuals known or suspected (for example via diagnose or symptoms) to be infected. In counterpart quarantine refers to the separation and detention of persons suspected to be infected or that have been exposed to an infectious agent(Barbera et al., 2001; Daubert, 2006; Cetron and Landwirth, 2005). Historically, quarantine interventions have proven to be effective on controlling Ebola outbreaks in Central Africa. Nonetheless, the unprecedented scale of the 2014 West African EVD outbreak joined to limited infrastructure poses a huge challenge on effectively implementing these control strategies. The main difference in modeling isolation and quarantine is incorporated in the way diagnosed individuals interact with the rest of the population. While individuals under quarantine are assumed still capable to interact with the rest of the population, without changing the population size in the force of infection term; individuals under isolation are incapable to interact with the rest of the population, impacting the population size. This two perspectives are usually reflected in the construction of the force of infection term (Brauer et al., 2001; Sattenspiel and Herring, 2003; Chowell and Nishiura, 2014).

In order to explore the effects of isolation and contrast them to the effects of quarantine, assume that a fraction r_i of the Patch i diagnosed individuals is isolated and cannot produce secondary infections, while the fraction of quarantined infected individuals $(1 - r_i)$ are ca-

pable to produce secondary infections at reduced infectiousness $l\beta$. According to model's (5.9) construction, the expected population sojourning in Patch i at time t is composed by the non-isolated Patch i individuals while at home $((1-t_i)(N_i - r_i J_i))$ and the non-quarantined Patch j individuals while spending time in Patch i $((1-q_j)t_j N_j)$. Simulations in Figure 5.6 contrast the effects of perfectly quarantine 30% of diagnosed pre-symptomatic individuals ($l_1 = 0$ and $r_1 = 0$) and isolate them ($l_1 = 0$ and $r_1 = 1$). For "low" mobility values isolation of pre-symptomatic infected individuals has an adverse effect on the total attack rate. This is exhibited in a bigger attack rate when diagnosed individuals are completely segregated.
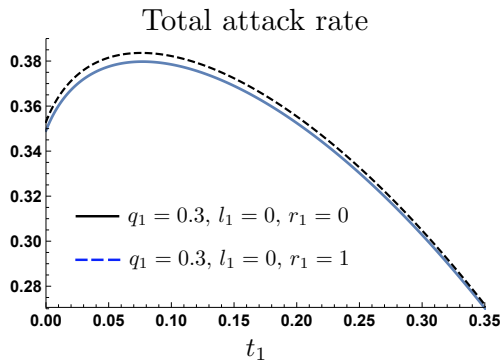
Figure 5.6: Effects of Patch 1 isolation on the total attack rate
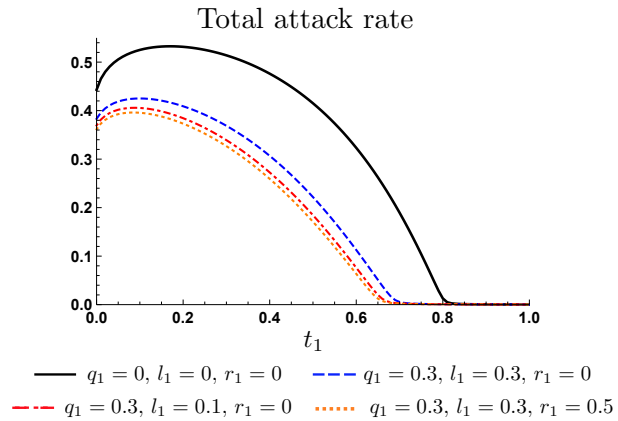
Figure 5.7: Effects of Patch 1 quarantine on the control of EVD

Figure 5.7 shows the total attack rate as function of Patch 1 mobility in the absence of any control measure ($q_1 = 0$, $l_1 = 0$, $r_1 = 0$), in the presence of quarantine reducing diagnosed pre-symptomatic individuals' infectiousness by 70% ($q_1 = 0.3$, $l_1 = 0.3$, $r_1 = 0$), in the presence of quarantine reducing diagnosed infectiousness by 90% ($q_1 = 0.3$, $l_1 = 0.1$, $r_1 = 0$), and in the presence of quarantine reducing diagnosed infectiousness by 70% and isolation of 50% of diagnosed individuals ($q_1 = 0.3$, $l_1 = 0.3$, $r_1 = 0$). Interestingly, increasing quarantine effectiveness from 70% to 90%, is not as effective as maintaining quarantine effectiveness at 70% and isolate 50% of pre-symptomatic diagnosed individuals.

Previous results show that under the scenario where a fraction of the infected population is quarantined, there exists a trade off between increasing quarantine effectiveness and completely isolate a fraction of the quarantined population. Further analysis would be required to completely disentangle dynamics of these control measures jointly acting on ameliorate the EVD burden.

5.5.3 The Joint Effect of High-Risk Region Quarantine and Traveling

In this section, the impact of Patch 1 control measures are numerically explored. To do so, Patch 2 is assumed to implement no control measures and residents are assumed avoid traveling to Patch 1. This work particularly focus on study the impact of quarantine on the *cordons sanitaires* traveling threshold and the mobility threshold leading the global basic reproductive number bellow one.

Figure 5.8 shows the curves along which mobility has no benefits over the *cordons sanitaires* scenario. The effects of quarantine programs in the high-risk region, is clearly seen on the increment of risk levels for which implementation of the *cordons sanitaires* is not the best strategy. For instance, $q_1 = 0$ implies that for $\mathscr{R}_{02} < 0.35$, all mobility regimes decreases the total attack rate, implying that implementation of the *cordons sanitaires* under these scenarios would be the worst decision. In counterpart, $q_1 = 0.15$ relaxes the sanitary conditions required in Patch 2, allowing the local basic reproductive number raising up to $\mathscr{R}_{02} \approx 0.5$ implying that the *cordons sanitaires* strategy would be avoided.
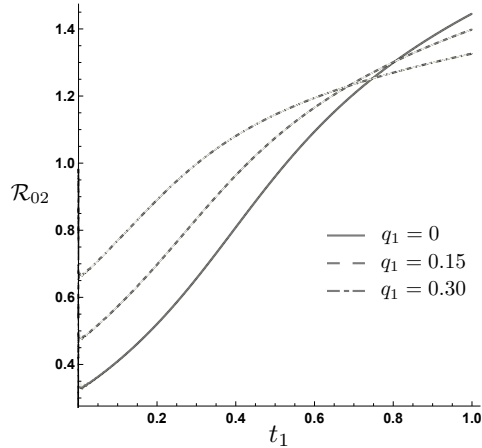
Figure 5.8: Effects of Patch 1 quarantine on the *cordons sanitaires* effectiveness
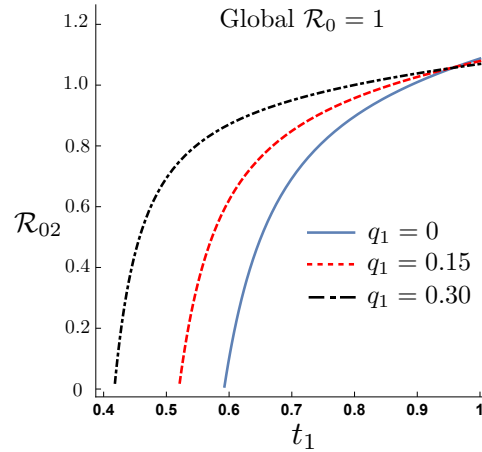
Figure 5.9: Effects of Patch 1 quarantine on the control of EVD

The EVD eradication mobility threshold is also highly sensitive to Patch 1 interventions. Figure 5.9 illustrates the level curves $\mathscr{R}_0(t_1, \mathscr{R}_{02}) = 1$, when 0%, 15% and 30% of Patch 1 pre-symptomatic individuals are isolated. According to simulations, in absence of Patch 2 mobility and quarantine, Patch 1 traveling can lead to eradication of an EVD outbreak whenever $\mathscr{R}_{02} < 1$. Furthermore, the required mobility to eradicate an EVD outbreak is reduced as more Patch 1 latent individuals are isolated. More interestingly increasing quarantine in Patch 1, sharpen the eradication mobility threshold, making it less sensitive to the Patch 2 risk of infection. On extreme scenarios, when at least 60% of Patch 1 pre-symptomatic individuals are isolated, the EVD outbreak control is independent of the traveling regime, see Figure 5.10. This result is consistent to the single patch scenario explored in Chapter 2, where results suggest that in order to control and EVD outbreak, a minimum of 60% pre-symptomatic individuals is required to be isolated.

Previous results showed that widely applied quarantine programs as well as relative "high" traveling levels can lead to the eventual control of an EVD outbreak. However, efforts to contain an eventual EVD outbreak by using a single control strategy might be daunting. Then, a strategy combining quarantine and mobility levels leading to the eradication of EVD in the affected regions might be appealing. In order to illustrate the joint

effect of Patch 1 mobility and quarantine, Figure 5.11 shows the impact of quarantine and mobility on the total attack rate, for a Patch 2 having a local infection risk of $\mathscr{R}_{02} = 0.9$.
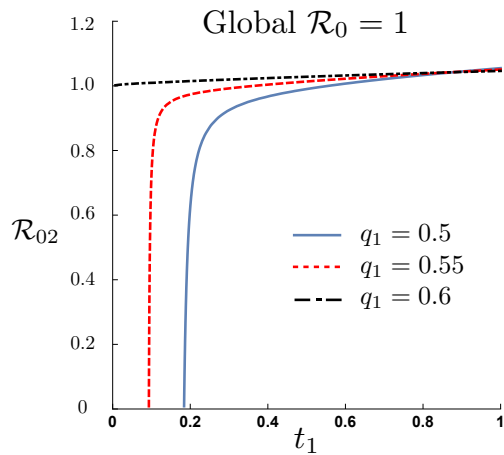
Figure 5.10: Effects of large Patch 1 quarantine programs on the control of EVD
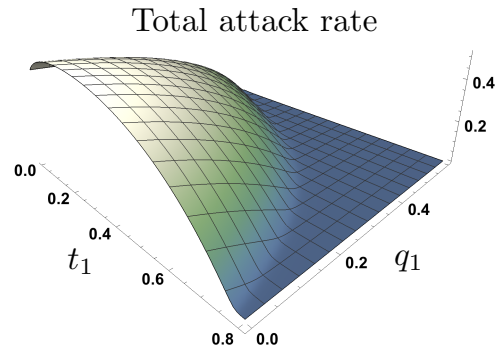
Figure 5.11: Total attack rate as function of Patch 1 traveling t_1 and quarantine q_1, for $\mathscr{R}_{02} \approx 0.9$.

Figure 5.12 shows the non-linear relation between quarantine and mobility required to reduce the total attack rate bellow the *cordons sanitaires* level. Increasing Patch 1 mobility produces that higher quarantine levels are required, attaining a maximum quarantine at $t_1 \approx 0.1$. This maximum turns out to be dependent on the Patch 2 risk of infection, as it is exhibited in Figure 5.13 for different Patch 2 risks of infection.
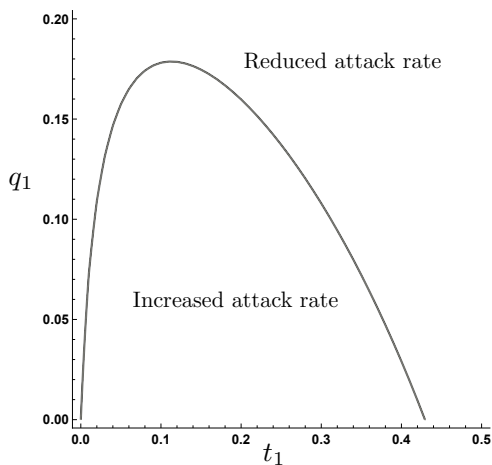
Figure 5.12: Level curve of the total attack rate on the plane (t_1, q_1), for the *cordons sanitaires* level.
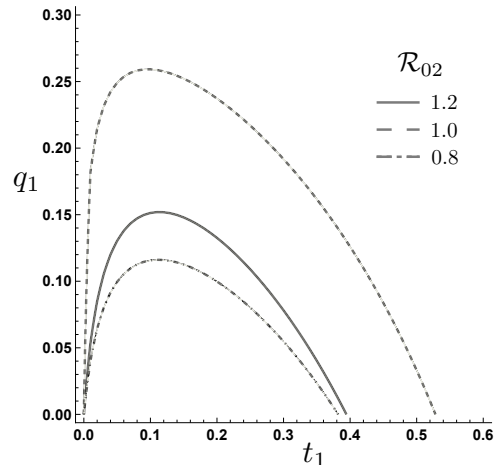
Figure 5.13: Patch 2 risk of infection defines the mobility-quarantine critical combination.

The non-monotonic behavior of the critical quarantine-mobility relation is generated by the reduced effect of mobility as $\mathscr{R}_{02}$ increases. This behavior can be explained geometrically by noticing that the "hump" on the total attack rate surface in Figure 5.11, gets smother as $\mathscr{R}_{02}$ diverges from one.

It is worth to stress that relative "small" mobility values producing an increment on the total attack rate demand wider quarantine in order to maintain the attack rate on the *cordons sanitaires* level. According to the presented model, high-risk residents spending around 10% of their time in the safe patch produce the worst impact, increasing the attack rate. This becomes relevant at the time of analyzing the efficiency of the *cordons sanitaires* strategy. Besides the controversy involved in the use of the *cordons sanitaires* during the 2014 West African EVD epidemic, produced mainly because this strategy is intended to stop the spread of the epidemic outside the cordoned region, without caring about the within population, the impossibility of perfectly contain individuals, produced a leakage turned out to be harmful for the EVD epidemic containment. The exhibited results are in agreement to the currently disentangled effects of the *cordons sanitaires*, seen during the 2014 EVD West African epidemic.

5.5.4   The Joint Effect of Low-Risk Region Quarantine and Traveling

Previous section showed that whenever $\mathscr{R}_{02} < 1$ an EVD epidemic can be contained by localized control measures implemented in the high-risk region. In this section the effects of Patch 2 quarantine on the control of EVD outbreak, when combined to Patch 1 quarantine and mobility, are explored.

Figure 5.14 shows the effect of quarantine Patch 2 pre-symptomatic individuals on the *cordons sanitaires* strategy effectiveness, in absence of Patch 1 interventions. Despite quarantined individuals residents of the low-risk zone has a moderate effect on decreasing the total attack rate, the dynamics of the *cordons sanitaires* threshold are heavily affected.
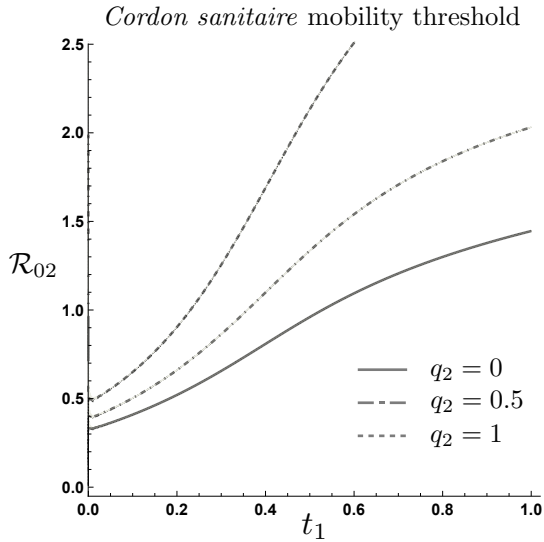
Figure 5.14: Impact of Patch 2 quarantine on the mobility needed to reduce the *cordons sanitaires* threshold
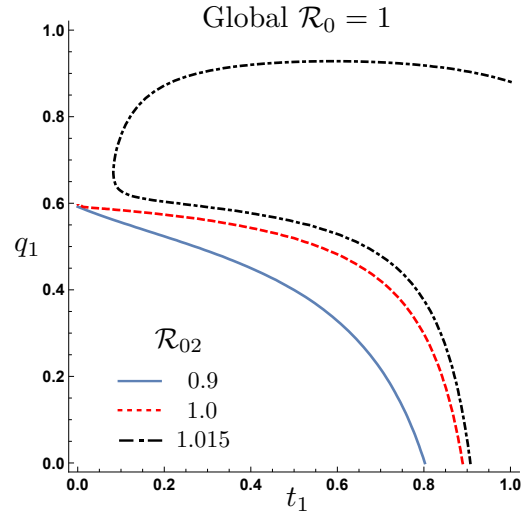
Figure 5.15: High-risk patch quarantine cannot eradicate an EVD outbreak if $\mathscr{R}_{02} > 1$

Figure 5.15 shows that whenever $\mathscr{R}_{02} < 1$, EVD eradication can be achieved by only quarantine individuals in Patch 1. Moreover, the safer Patch 2, the major the mobility effect on reducing the quarantine needed con take the global $\mathscr{R}_0$ bellow one. For instance, the scenario of an $\mathscr{R}_{02} = 0.9$ and $t_1 \approx 0.5$, would require to quarantine around 40% of Patch 1 pre-symptomatic individuals; while an $\mathscr{R}_{02} = 1$ under the same mobility level would require to quarantine around 50% of the infected population. Furthermore, for $\mathscr{R}_{02}$ slightly greater than one, the combination of Patch 1 quarantine and traveling, is capable to lead to the eventual eradication of an EVD outbreak. For example, under the scenario $\mathscr{R}_{02} = 1.015$, Patch 1 quarantine is not enough to take the control reproductive number bellow one. In this case, a combined strategy of mobility of $t_1 \approx 0.15$ and quarantine between 60% to 90% would lead to EVD eradication. This exhibits the impact of big quarantine programs on reducing the traveling population, and in consequence, the impact of traveling management as a control strategy. In Figure 5.15, the extreme scenario of quarantining above 90% of pre-symptomatic individuals, reduces enough the traveling population, so that there is no mobility regime capable to lead to the EVD eradication, in absence of Patch 2 interventions.

79

5.6   Discussion

In this chapter it was shown that under the simple scenario of two regions with differential Ebola Virus Disease (EVD) infection risk, the joint use of mobility and localized control measures might be an appealing strategy in order to properly manage the EVD spread on the whole system. Results show that, control measures applied in the high-risk region have major impacts than those implemented in the low-risk region. Nonetheless, this does not mean that having good sanitary conditions in the safe region is not important. If mobility would be used as a control strategy, sanitary conditions of both patches are important. The trade off between increasing quarantine effectiveness or increase the fraction of isolated diagnosed pre-symptomatic individuals was briefly addressed via numerical simulations. Results show that more analysis is required in order to accurately assess the impact of each control strategy under an EVD epidemic. Either quarantine or isolate a large proportion of the population, directly impacts the effective population traveling and/or the effective population sojourning in a given patch. Results show that the joint implementation of quarantine and mobility control strategies require further analysis in order to properly address the potential beneficial and harmful effects of joint implementation of these control strategies.

Chapter 6

CONCLUSIONS & DISCUSSION

The 2014 West African Ebola Virus Disease (EVD) epidemic, after the 2003 Severe Acute
Respiratory Syndrome (SARS) epidemic and 2009 influenza A (H1N1) pandemic, dis-
closed a highly connected world with enormous potential to rapidly spread a disease world-
wide. Fast and accessible transportation around the world doubtless produces invaluable
benefits in many aspects, but at the same time generating interdependence across nations
and posing new global challenges. The West African epidemic showed that currently a
virus can worldwide spread in few hours, the same period for an infected individual to
develop symptoms. The imported EVD case in Lagos, Nigeria, by an international flight
from Liberia, is but an example of such international threat. In this work, the role of
highly vulnerable regions as the weakest link in a global health system is assessed. These
regions, where spillover events are highly likely to happen, are critical for early disease
containment. Unpreparedness of these regions facilitates conditions for a local outbreak to
become a serious international problem, as seen in the 2014 West African EVD epidemic.
The presented work envisioned the EVD affected region as a polarized area to study the
effects of risk heterogeneity on the dynamics of EVD. The introduction of the Lagrangian
modeling approach to study the EVD dynamics is useful in many aspects, as it makes use
of measurable parameters (infection risk and residency time, for instance) and as EVD
dynamics can be locally (this is, patch-specific) and globally (over the two patch system)
assessed. The metrics used in this works includes the local and global (the two patch sys-
tem) basic reproductive number and final epidemic sizes as functions of the patch specific
mobility, infection risks and density. The main contributions of the presented work are
done around the potential benefits of mobility management as a control measure. Particu-

larly, across regions exhibiting extreme differences on health care access, disease risks and population's densities. The derived results challenge the stigmatized classical notion of population mobility as producing a harmful effect on the containment of an epidemic. The *cordons sanitaires*' effectiveness was assessed as function of the mobility, patch-specific risk of infection and patch density.

Results suggest that three scenarios characterize the *cordons sanitaires*' effectiveness in terms of the total final number of EVD-infected individuals: a very safe neighboring region implies that travel ban is the worst decision as a control measure, an "intermediate" safe neighboring region conditions the *cordons sanitaires*' effectiveness on specific mobility levels after which the final epidemic size reduces, and a relatively "high risk" neighboring region for which the *cordons sanitaires* strategy appears to be the best control strategy. Moreover, the dynamics of the threshold condition for EVD eradication in terms of the patch population mobility is assessed in terms of its dependence on the patch-specific infection risk and implementation of localized control strategies. Finally, the impact of patch-specific density on the dynamics of the mobility threshold reducing the total final epidemic size (compared to the *cordons sanitaires* scenario) and the mobility threshold required to properly manage EVD are explored.

The simple setting used in the present work seems able to shed light on the EVD dynamics exhibited in the zone divided by a *cordons sanitaires* barrier. However, the appropriate minimum number of patches needed to capture the dynamics of specific systems should be addressed. The proposed problem, although in principle, similar to the problem of the minimum number of pixels required to gain the best image quality at different scales, is still more challenging. In the epidemiological context, the patch problem deals with humans changing their behaviors according to their threat's perception. Thus, not only the number of patches to be incorporated has a critical role in the study of epidemic's dynamics, but also the role of human behavior becomes imperative.

The many factors combined in West Africa promoting an event of global scale had different nature. Social characteristics like population's fear and government distrust, poor coordination at distinct levels, as well as people's reluctance to suspend traditional practices, among others; extreme poverty reflected in lack of appropriate health system infrastructure, basic medical supplies and insufficient personal protective equipment; and, highly connectivity between the West African communities and, its proximity to highly dense cities, are but some factors that deeply influenced the course of the outbreak. Many of the control measures implemented during the 2014 West African outbreak can be identified as temporary effective, i.e feasible in presence of international aid, but not sustainable without it. Contact tracing, besides its high implementation costs, becomes challenging and less effective in presence of mobility. On the other hand, high isolation effectiveness is required to produce a significant impact on the EVD control, moreover, this control measure is highly dependent on treatment center capacity and transportation availability. Robust control measures, planned to effectively persist beyond the crisis period, might be expensive at the implementation time, but doubtless represent the best investment over time. The outcome of maintain inequalities across nations or cities, might ultimately be more expensive than start investing on sustainable control measures. For instance, in the case of zoonotic diseases, beyond the complex task that eradication of the wild carrier would represent, a species eradication might dramatically alter a whole ecosystem, potentially triggering a worst event. The consequences of altering an ecosystem has been documented in many scenarios, for example the wolfs reintroduction in the Yellowstone park and the incredible change in the whole ecosystem and geography. Such environmental complexity demand us to safely coexist with the countless disease agents we are continuously exposed to. On the other hand, it is well known that decisions are made on individual's risk perception and directly affected by the event probability. However, decisions made towards increasing the contrast between the privileged and the oppressed, can ultimately lead us towards

83

a global disastrous scenario. The impossibility of preventing the next spillover demand us to identify the real goal as not only be capable to contain an ongoing outbreak, but as being capable to design a global strong public health system. In retrospective, it is not hard to see that enhancement of health care systems in the highly affected regions, along with implementation of sustainable control measures aimed to vanishing existing inequalities, would be the path to attain a global strong health system. Nonetheless, this will be possible until global engagement on international public health preparedness occurs, otherwise we might continuously experiencing local outbreaks becoming international public health treats. In the end, it is our ethical responsibility to construct moral based policies equally caring about people's health, regardless their nationality, race, ethnics and other personal characteristics.

Bibliography

A. Maxmen (2017). Ebola vaccine approved for use in ongoing outbreak.

ABC News (2014). Ebola crisis: Sierra leone hit by largely hidden outbreak; who says scores of bodies piled up.

Agence France-Presse (2018). Ebola-hit african states seal off outbreak epicentre.

Althaus, C. L. (2014). Estimating the reproduction number of ebola virus (ebov) during the 2014 outbreak in west africa. *PLoS currents*, 6.

Amesh Adalja (2018). Quarantining an entire liberian slum to fight ebola is a recipe for disaster.

Ansumana, R., Jacobsen, K. H., Idris, M., Bangura, H., Boie-Jalloh, M., Lamin, J. M., Sesay, S., and Sahr, F. (2015). Ebola in freetown area, sierra leone—a case study of 581 patients. *New England Journal of Medicine*, 372(6):587–588.

Arino, J. and Van Den Driessche, P. (2003). The basic reproduction number in a multi-city compartmental epidemic model. In *Positive Systems*, pages 135–142. Springer.

Arino, J. and Van den Driessche, P. (2006). Disease spread in metapopulations. *Nonlinear dynamics and evolution equations*, 48:1–13.

Baize, S., Pannetier, D., Oestereich, L., Rieger, T., Koivogui, L., Magassouba, N., Soropogui, B., Sow, M. S., Keïta, S., De Clerck, H., et al. (2014). Emergence of zaire ebola virus disease in guinea. *New England Journal of Medicine*, 371(15):1418–1425.

Barbera, J., Macintyre, A., Gostin, L., Inglesby, T., O'toole, T., DeAtley, C., Tonat, K., and Layton, M. (2001). Large-scale quarantine following biological terrorism in the united states: scientific examination, logistic and legal limits, and possible consequences. *Jama*, 286(21):2711–2717.

BBC News (2018). Who: Ebola 'an international emergency'.

Bichara, D. and Castillo-Chavez, C. (2016). Vector-borne diseases models with residence times–a lagrangian perspective. *Mathematical biosciences*, 281:128–138.

Bichara, D. and Iggidr, A. (2017). Multi-patch and multi-group epidemic models: a new framework. *Journal of mathematical biology*, pages 1–28.

Bichara, D., Kang, Y., Castillo-Chavez, C., Horan, R., and Perrings, C. (2015). Sis and sir epidemic models under virtual dispersal. *The Bulletin of Mathematical Biology, DOI: 10.1007/s11538-015-0113-5*.

Blackwood, J. and Childs, L. (2016). The role of interconnectivity in control of an ebola epidemic. *Scientific reports*, 6:29262.

Borio, L. L., Inglesby, T. V. ., Peters, C. J., Schmaljohn, A. L., Hughes, J., Jahrling, P. B., Ksiazek, T. G., Johnson, K. M., Meyerhoff, A., O'Toole, T., Ascher, M. S., Bartlett, J. G. ., Breman, J. G., Eitzen, E. M., Hamburg, M. A., Hauer, J., Henderson, D. A., Johnson, R. T., Kwik, G., Layton, M., Lillibridge, S. R., Nabel, G. J., Osterholm, M. T., Perl, T., Russell, P. K., and Tonat, K. (2002). Hemorrhagic fever viruses as biological weapons: medical and public health management. *JAMA*, 287 18:2391–405.

Bowen, E., Platt, G., Lloyd, G., Baskerville, A., Harris, W., Vella, E., et al. (1977). Viral haemorrhagic fever in southern sudan and northern zaire. preliminary studies on the aetiological agent. *Lancet*, pages 571–573.

Brauer, F., Castillo-Chavez, C., and Castillo-Chavez, C. (2001). *Mathematical models in population biology and epidemiology*, volume 40. Springer.

Breman, J. G., Arita, I., Unit, S. E., Organization, W. H., et al. (1980). The confirmation and maintenance of smallpox eradication.

Bruce, J. and Brysiewicz, P. (2002). Ebola fever: the african emergency. *International journal of trauma nursing*, 8(2):36–41.

Castillo-Chavez, C., Bichara, D., and Morin, B. R. (2016). Perspectives on the role of mobility, behavior, and time scales in the spread of diseases. *Proceedings of the National Academy of Sciences*, 113(51):14582–14588.

Castillo-Chavez, C., Song, B., and Zhangi, J. (2003). An epidemic model with virtual mass transportation: The case of smallpox. *Bioterrorism: Mathematical Modeling Applications in Homeland Security*, 28:173.

CDC, C. f. D. C. (2017). Bioterrorism agents/diseases.

CDC, C. f. D. C. (2018a). 2014-2016 ebola outbreak in west africa.

CDC, C. f. D. C. (2018b). Ebola (ebola virus disease).

CDC, C. f. D. C. (2018c). Importance of communication in outbreak response: Ebola.

CDC, C. f. D. C. (2018d). Preliminary study finds that ebola virus fragments can persist in the semen of some survivors for at least nine months.

CDC, C. f. D. C. (2018e). Recommendations for breastfeeding/infant feeding in the context of ebola virus disease.

Cetron, M. and Landwirth, J. (2005). Public health and ethical considerations in planning for quarantine. *The Yale journal of biology and medicine*, 78(5):329.

Chowell, D., Castillo-Chavez, C., Krishna, S., Qiu, X., and Anderson, K. S. (2015). Modelling the effect of early detection of ebola. *The Lancet Infectious Diseases*, 15(2):148–149.

Chowell, G., Hengartner, N. W., Castillo-Chavez, C., Fenimore, P. W., and Hyman, J. (2004). The basic reproductive number of ebola and the effects of public health measures: the cases of congo and uganda. *Journal of theoretical biology*, 229(1):119–126.

Chowell, G. and Nishiura, H. (2014). Transmission dynamics and control of ebola virus disease (evd): a review. *BMC medicine*, 12(1):196.

Chughtai, A., Barnes, M., and Macintyre, C. (2016). Persistence of ebola virus in various body fluids during convalescence: evidence and implications for disease transmission and control. *Epidemiology & Infection*, 144(8):1652–1660.

Coltart, C. E., Lindsey, B., Ghinai, I., Johnson, A. M., and Heymann, D. L. (2017). The ebola outbreak, 2013–2016: old lessons for new epidemics. *Phil. Trans. R. Soc. B*, 372(1721):20160297.

Commission, I. et al. (1978). Ebola haemorrhagic fever in zaire, 1976. *Bull World Health Organ*, 56(2):271–293.

Daubert, M. A. (2006). Pandemic fears and contemporary quarantine: protecting liberty through a continuum of due process rights. *Buff. L. Rev.*, 54:1299.

Deen, G. F., Broutet, N., Xu, W., Knust, B., Sesay, F. R., McDonald, S. L., Ervin, E., Marrinan, J. E., Gaillard, P., Habib, N., et al. (2017). Ebola rna persistence in semen of ebola virus disease survivors. *New England Journal of Medicine*, 377(15):1428–1437.

Diallo, B., Sissoko, D., Loman, N. J., Bah, H. A., Bah, H., Worrell, M. C., Sacko, R., Mesfin, S., Loua, A., Kalonda, J. K., et al. (2016). Resurgence of ebola virus disease in guinea linked to a survivor with virus persistence in seminal fluid for more than 500 days. *Clinical infectious diseases*, 63(10):1353–1356.

Diekmann, O., Heesterbeek, J. A. P., and Metz, J. A. J. (1990). On the definition and the computation of the basic reproduction ratio R_0 in models for infectious diseases in heterogeneous populations. *J. Math. Biol.*, 28(4):365–382.

E. Callaway (2017). Successful ebola vaccine provides 100

Espinoza, B., Moreno, V., Bichara, D., and Castillo-Chavez, C. (2016). Assessing the efficiency of movement restriction as a control strategy of ebola. In *Mathematical and Statistical Modeling for Emerging and Re-emerging Infectious Diseases*, pages 123–145. Springer.

Eubank, S., Guclu, H., Kumar, V. A., Marathe, M. V., Srinivasan, A., Toroczkai, Z., and Wang, N. (2004). Modelling disease outbreaks in realistic urban social networks. *Nature*, 429(6988):180–184.

Falasca, L., Agrati, C., Petrosillo, N., Di Caro, A., Capobianchi, M., Ippolito, G., and Piacentini, M. (2015). Molecular mechanisms of ebola virus pathogenesis: focus on cell death. *Cell death and differentiation*, 22(8):1250.

Feldmann, H. (2010). Are we any closer to combating ebola infections? *Lancet*, 375(9729):1850.

Feldmann, H. and Geisbert, T. W. (2011). Ebola haemorrhagic fever. *The Lancet*, 377(9768):849–862.

Feldmann, H., Wahl-Jensen, V., Jones, S. M., and Ströher, U. (2004). Ebola virus ecology: a continuing mystery. *Trends in microbiology*, 12(10):433–437.

Fowler, R. A., Fletcher, T., Fischer, W. A., Lamontagne, F., Jacob, S., Brett-Major, D., Lawler, J. V., Jacquerioz, F. A., Houlihan, C., O'Dempsey, T., et al. (2014). Caring for critically ill patients with ebola virus disease. perspectives from west africa. *American journal of respiratory and critical care medicine*, 190(7):733–737.

Gire, S. K., Goba, A., Andersen, K. G., Sealfon, R. S., Park, D. J., Kanneh, L., Jalloh, S., Momoh, M., Fullah, M., Dudas, G., et al. (2014). Genomic surveillance elucidates ebola virus origin and transmission during the 2014 outbreak. *science*, page 1259657.

Gomes, M. F., y Piontti, A. P., Rossi, L., Chao, D., Longini, I., Halloran, M. E., and Vespignani, A. (2014). Assessing the international spreading risk associated with the 2014 west african ebola outbreak. *PLoS currents*, 6.

Hewlett, B. S. and Amola, R. P. (2003). Cultural contexts of ebola in northern uganda. *Emerging infectious diseases*, 9(10):1242.

Iggidr, A., Sallet, G., and Souza, M. O. (2016). On the dynamics of a class of multi-group models for vector-borne diseases. *Journal of Mathematical Analysis and applications*, 441(2):723–743.

Johnson, K., Webb, P., Lange, J., Murphy, F., et al. (1977). Isolation and partial characterisation of a new virus causing acute haemorrhagic fever in zaire. *Lancet*, pages 569–571.

Keeling, M. J. (1999). The effects of local spatial structure on epidemiological invasions. *Proceedings of the Royal Society of London B: Biological Sciences*, 266(1421):859–867.

Kucharski, A. J., Camacho, A., Flasche, S., Glover, R. E., Edmunds, W. J., and Funk, S. (2015). Measuring the impact of ebola control measures in sierra leone. *Proceedings of the National Academy of Sciences*, 112(46):14366–14371.

Kuhn, J. H., Becker, S., Ebihara, H., Geisbert, T. W., Johnson, K. M., Kawaoka, Y., Lipkin, W. I., Negredo, A. I., Netesov, S. V., Nichol, S. T., et al. (2010). Proposal for a revised taxonomy of the family filoviridae: classification, names of taxa and viruses, and virus abbreviations. *Archives of virology*, 155(12):2083–2103.

Legrand, J., Grais, R. F., Boelle, P.-Y., Valleron, A.-J., and Flahault, A. (2007). Understanding the dynamics of ebola epidemics. *Epidemiology & Infection*, 135(4):610–621.

Leroy, E. M., Baize, S., Volchkov, V., Fisher-Hoch, S., Georges-Courbot, M., Lansoud-Soukate, J., Capron, M., Debre, P., Georges, A., and McCormick, J. (2000). Human asymptomatic ebola infection and strong inflammatory response. *The Lancet*, 355(9222):2210–2215.

Li, J., Duan, H.-J., Chen, H.-Y., Ji, Y.-J., Zhang, X., Rong, Y.-H., Xu, Z., Sun, L.-J., Zhang, J.-Y., Liu, L.-M., et al. (2016). Age and ebola viral load correlate with mortality and survival time in 288 ebola virus disease patients. *International Journal of Infectious Diseases*, 42:34–39.

Matua, G. A., Wal, D. M. V. d., and Locsin, R. C. (2015). Ebola hemorrhagic fever outbreaks: strategies for effective epidemic management, containment and control. *Brazilian Journal of Infectious Diseases*, 19(3):308–313.

Moreno, V., Espinoza, B., Barley, K., Paredes, M., Bichara, D., Mubayi, A., and Castillo-Chavez, C. (2017a). The role of mobility and health disparities on the transmission dynamics of tuberculosis. *Theoretical Biology and Medical Modelling*, 14(1):3.

Moreno, V. M., Espinoza, B., Bichara, D., Holechek, S. A., and Castillo-Chavez, C. (2017b). Role of short-term dispersal on the dynamics of zika virus in an extreme idealized environment. *Infectious Disease Modelling*, 2(1):21–34.

Mossong, J., Hens, N., Jit, M., Beutels, P., Auranen, K., Mikolajczyk, R., Massari, M., Salmaso, S., Tomba, G. S., Wallinga, J., et al. (2008). Social contacts and mixing patterns relevant to the spread of infectious diseases. *PLoS medicine*, 5(3):e74.

Ndambi, R., Akamituna, P., Bonnet, M.-J., Tukadila, A. M., Muyembe-Tamfum, J.-J., and Colebunders, R. (1999). Epidemiologic and clinical aspects of the ebola virus epidemic in mosango, democratic republic of the congo, 1995. *The Journal of infectious diseases*, 179(Supplement_1):S8–S10.

Nelson, K. E. and Williams, C. (2013). *Infectious disease epidemiology*. Jones & Bartlett Publishers.

of a WHO/International Study Team, R. et al. (1978). Ebola haemorrhagic fever in sudan, 1976. *Bulletin of the World Health Organization*, 56(2):247.

ONISHI, N. (2014). As ebola grips liberia's capital, a quarantine sows social chaos.

Pandey, A., Atkins, K. E., Medlock, J., Wenzel, N., Townsend, J. P., E, C. J., Nyenswah, T. G., Ndeffo-Mba, M. L., and Galvani, A. P. (2014). Strategies for containing ebola in west africa.

Piot, P., Muyembe, J.-J., and Edmunds, W. J. (2014). Ebola in west africa: from disease outbreak to humanitarian crisis. *The Lancet Infectious Diseases*, 14(11):1034–1035.

Polesky, A. and Bhatia, G. (2003). Ebola hemorrhagic fever in the era of bioterrorism. In *Seminars in respiratory infections*, volume 18, pages 206–215.

Pourrut, X., Kumulungui, B., Wittmann, T., Moussavou, G., Délicat, A., Yaba, P., Nkoghe, D., Gonzalez, J.-P., and Leroy, E. M. (2005). The natural history of ebola virus in africa. *Microbes and infection*, 7(7-8):1005–1014.

R. K. Hoffmann et.al (2018). Ethical considerations in the use of cordons sanitaires.

Sattenspiel, L. and Dietz, K. (1995). A structured epidemic model incorporating geographic mobility among regions. *Mathematical biosciences*, 128(1-2):71–91.

Sattenspiel, L. and Herring, D. A. (2003). Simulating the effect of quarantine on the spread of the 1918–19 flu in central canada. *Bulletin of mathematical biology*, 65(1):1–26.

Sorichetta, A., Bird, T. J., Ruktanonchai, N. W., zu Erbach-Schoenberg, E., Pezzulo, C., Tejedor, N., Waldock, I. C., Sadler, J. D., Garcia, A. J., Sedda, L., et al. (2016). Mapping internal connectivity through human migration in malaria endemic countries. *Scientific data*, 3:160066.

Stroud, P., Del Valle, S., Sydoriak, S., Riese, J., and Mniszewski, S. (2007). Spatial dynamics of pandemic influenza in a massive artificial society. *Journal of Artificial Societies and Social Simulation*, 10(4):9.

Team, W. E. R. (2014). Ebola virus disease in west africa—the first 9 months of the epidemic and forward projections. *New England Journal of Medicine*, 371(16):1481–1495.

Towers, S., Patterson-Lomba, O., and Castillo-Chavez, C. (2014). Temporal variations in the effective reproduction number of the 2014 west africa ebola outbreak. *PLoS currents*, 6.

Towner, J. S., Rollin, P. E., Bausch, D. G., Sanchez, A., Crary, S. M., Vincent, M., Lee, W. F., Spiropoulou, C. F., Ksiazek, T. G., Lukwiya, M., et al. (2004). Rapid diagnosis of ebola hemorrhagic fever by reverse transcription-pcr in an outbreak setting and assessment of patient viral load as a predictor of outcome. *Journal of virology*, 78(8):4330–4341.

UN, U. N. (2018). Ebola response.

Van den Driessche, P. (2008). Spatial structure: patch models. In *Mathematical epidemiology*, pages 179–189. Springer.

van den Driessche, P. and Watmough, J. (2002). reproduction numbers and sub-threshold endemic equilibria for compartmental models of disease transmission. *Math. Biosci.*, 180:29–48.

Wesolowski, A., Eagle, N., Tatem, A. J., Smith, D. L., Noor, A. M., Snow, R. W., and Buckee, C. O. (2012). Quantifying the impact of human mobility on malaria. *Science*, 338(6104):267–270.

WHO (2018). Factors that contributed to undetected spread of the ebola virus and impeded rapid containment.

WHO, W. H. O. (2015). Ebola virus disease.